

QBOi El Niño Southern Oscillation experiments: Assessing relationships between ENSO, MJO, and QBO

Dillon Elsbury^{1,2}, Federico Serva³, Julie M. Caron⁴, Seung-Yoon Back⁵, Clara Orbe⁶, Jadwiga H. Richter⁴, James A. Anstey⁷, Neal Butchart⁸, Chih-Chieh Chen⁴, Javier García-Serrano^{9,10}, Anne Glanville⁴, Yoshio Kawatani^{11,12}, Tobias Kerzenmacher¹³, Francois Lott¹⁴, Hiroaki Naoe¹⁵, Scott Osprey^{16,17}, Froila M. Palmeiro^{9,18}, Seok-Woo Son⁵, Masakazu Taguchi¹⁹, Stefan Versick¹³, Shingo Watanabe²⁰, Kohei Yoshida¹⁵

¹ Cooperative Institute for Research in Environmental Sciences University of Colorado Boulder, Boulder, Colorado, USA

² NOAA/Chemical Sciences Laboratory, Boulder, Colorado, USA

³ Institute of Marine Sciences, National Research Council (ISMAR-CNR), Rome, Italy

⁴ U. S. National Science Foundation National Center for Atmospheric Research (NSF NCAR), Boulder, CO, USA

⁵ School of Earth and Environmental Sciences, Seoul National University, Seoul, South Korea

⁶ NASA Goddard Institute for Space Studies (GISS), New York, New York, USA

⁷ Canadian Centre for Climate Modelling and Analysis (CCCma), Victoria, British Columbia, Canada

⁸ Met Office Hadley Centre, Exeter, United Kingdom

⁹ Group of Meteorology, Universitat de Barcelona, Barcelona, Spain

¹⁰ Barcelona Supercomputing Center (BSC), Barcelona, Spain

¹¹ Faculty of Environmental Earth Science, Hokkaido University, Sapporo, Japan

¹² Japan Agency for Marine-Earth Science and Technology, Yokohama, Japan

¹³ Institute of Meteorology and Climate Research-Atmospheric Trace Gases and Remote Sensing (IMK-ASF) Karlsruhe Institute of Technology (KIT), Karlsruhe, Germany

¹⁴ Laboratoire de Météorologie Dynamique (LMD), Paris, France

¹⁵ Meteorological Research Institute (MRI), Tsukuba, Japan

¹⁶ National Centre for Atmospheric Science (NCAS), United Kingdom

¹⁷ Department of Physics, University of Oxford, United Kingdom

43
44 ¹⁸ CMCC Foundation - Euro-Mediterranean Center on Climate Change, Italy

45
46 ¹⁹ Aichi University of Education, Kariya, Japan

47
48 ²⁰ Japan Agency for Marine-Earth Science and Technology (JAMSTEC), Yokohama, Japan

49
50
51 *Correspondence to:* Dillon Elsbury (delsbury@uci.edu)

52 **Abstract.** This study uses an ensemble of climate model experiments coordinated by the Quasi-Biennial Oscillation initiative
53 (QBOi) to analyze the Madden-Julian Oscillation (MJO) in the presence of either perpetual El Niño or La Niña sea surface
54 temperatures during boreal winter. In addition to the prescribed El Niño Southern Oscillation (ENSO) conditions, the nine
55 models internally generate QBOs, meaning each may influence the MJO. [Objectives of our analyses are to assess the response](#)
56 [of the MJO to strong idealized ENSO forcing and look for evidence of a QBO influence on the MJO in a multi-model context.](#)
57 The diagnostics used include wavenumber-frequency spectra of tropical convective and dynamical fields, measures of MJO
58 lifetime, an evaluation of MJO diversity and visualization of MJO vertical structure, as well as an assessment of QBO
59 morphology and the QBO’s impact on tropical convection. Kelvin wave spectral power increases in the El Niño simulations
60 whereas equatorial Rossby waves power is stronger in the La Niña simulations. [All models simulate faster MJO propagation](#)
61 [under El Niño conditions.](#) This change in speed is corroborated by the MJO diversity analysis, which reveals that models better
62 reproduce the observed “fast propagating” and “standing” MJO archetypes given perpetual El Niño and La Niña, respectively.
63 Regardless of ENSO, QBO descent into the lower stratosphere is underestimated and we detect little QBO influence on tropical
64 tropopause stability and MJO activity. With little influence from the QBO on the MJO activity in these runs, we can be
65 confident that the aforementioned changes in the MJO indeed arise from the different ENSO boundary conditions.

66 **1 Introduction**

67 The tropical circulation is influenced by various forms of internal variability, each operating at different timescales, yet still
68 influencing each other. The Madden-Julian Oscillation (MJO) is dominant at intraseasonal timescales (Madden and Julian
69 1994; Lin, 2022). It consists of large-scale eastward propagating fluctuations in tropical precipitation and circulation that
70 traverse the Indian Ocean and Maritime Continent through to the Pacific over roughly 30 to 60 days (Hendon and Salby 1994).
71 MJO variability fluctuates a lot year to year as does other variability in the climate system.

72
73 At interannual timescales, the El Niño Southern Oscillation (ENSO; Philander, 1990) is one of the most consequential sources
74 of tropical tropospheric variability. It is characterized by shifting patterns of sea surface temperatures (SSTs) and associated
75 changes in ocean and atmospheric circulations in the tropical Pacific. ENSO varies on timescales between two to seven years,
76 and consists of three phases, the warm El Niño, the cold La Niña and a “neutral” phase where neither polarity dominates. Also

Formatted: Header

Deleted: dillon.elsbury@noaa.gov

Formatted: Font color: Text 1

Formatted: Font color: Text 1

Deleted: Consistent with the reported relationship between these waves and the MJO, all

Formatted: Header

operating at interannual timescales is the Quasi Biennial Oscillation (QBO), which is the dominant mode of variability in the lower tropical stratosphere, defined by alternating easterly and westerly shear zones descending from 5 to 100 hPa with an average periodicity of 28 months (Baldwin et al. 2001).

The MJO, ENSO, and QBO are known to influence each other in various ways. ENSO's La Niña and El Niño phases are associated with shifts of intraseasonal tropical atmospheric variability like the MJO towards the Indo-Pacific Warm Pool and Date Line, respectively (Kessler 2001; Tam and Lau 2005). In addition, ENSO can influence the amount of time the MJO spends in particular Wheeler and Hendon (2004) MJO phases and the duration of MJO events overall, which are shorter during El Niño and longer during La Niña (Pohl and Matthews 2007; Pang et al. 2016; Wei and Ren 2019; Wang et al. 2019; Dasgupta et al. 2021; Fernandes and Grimm 2023).

Nonetheless, not all research finds strong links between ENSO and seasonal-mean MJO activity. Slingo et al. (1999) found that the observed intraseasonally filtered zonal mean 200 hPa zonal wind (their metric of "MJO activity") is weakly dependent on ENSO phase. They affirmed this further by using an ensemble of AMIP simulations. Hendon et al. (1999) validated and refined their definition of MJO activity, finding it to capture the salient features of the MJO and again that its variability is mostly independent of ENSO. These results also align with those of Newman et al. (2009) who showed that air-sea coupling has a small effect on intraseasonal atmospheric variability in empirical models that run with and without atmosphere-ocean interaction. With these results in mind, it is less clear how the MJO should respond to the ENSO conditions prescribed in our simulations. In fact, a common idea amongst the studies just mentioned is that the MJO's interannual variability originates predominantly from internal atmospheric processes other than those associated with ENSO.

It is increasingly recognized that the easterly and westerly phases of the QBO exert an influence on the MJO (Yoo and Son, 2016; Son et al. 2017; Sakaeda et al. 2020; Martin et al. 2021; Jin et al. 2023; Huang et al. 2023). The MJO's amplitude is stronger during easterly QBO boreal winters compared to westerly QBO winters over the observed record since 1979 (Yoo and Son 2016; Densmore et al. 2019). However, despite improvement in the representation of simulated QBOs (Richter et al. 2020) and MJOs (Ahn et al. 2020) across model generations, current [free-running](#) Earth system models generally do not simulate the QBO-MJO relationship (Kim et al. 2020; Lim and Son 2020; Martin et al. 2023), nor do they simulate a sufficiently strong tropical tropopause response to the QBO (Serva et al. 2022). Further complicating interpretation is a tendency for easterly QBO boreal winters to co-occur with La Niña events, introducing ambiguity about the source of MJO modulation (Randall et al. 2023).

In this study, we document the influence of ENSO on the MJO using a multi-model ensemble of idealized experiments with perpetual El Niño and La Niña forcings. These simulations were coordinated by the Atmospheric Processes And their Role in Climate (APARC, previously "SPARC") Quasi-Biennial Oscillation initiative (QBOi; Butchart et al. 2018). In addition to

Formatted: Font color: Text 1

Formatted: Font color: Text 1

Deleted:), which seeks to improve the fidelity of tropical stratospheric variability in general circulation and Earth system models through coordinated multi-institutional climate model experiments (

Formatted: Font color: Text 1

118 prescribing ENSO, the models internally generate QBOs, meaning both types of interannual internal variability may modulate
 119 the MJO in these experiments. Our aim is to assess the extent to which model behavior is consistent with previously reported
 120 ENSO-MJO relationships, recognizing that past studies have found different ENSO-MJO links and that the simulated QBOs
 121 may also project onto the MJOs. The coordinated QBOi protocol allows us to revisit these relationship in a controlled
 122 framework that isolates atmospheric responses to fixed, high-amplitude ENSO SSTs across many models. These perpetual
 123 ENSO conditions represent the strongest observed El Niños and La Niñas and offer an upper bound on ENSO’s effect on MJO
 124 characteristics, providing a high signal-to-noise database for studying this connection. We also selectively incorporate Phase
 125 1 QBOi experiments, performed as 1979-2009 Atmospheric Model Intercomparison Project experiments, and hence, more
 126 representative of typical ENSO amplitudes (Butchart et al. 2018, Experiment 1). Unlike Coupled or Atmospheric Model
 127 Intercomparison Project experiments, or historical reanalysis datasets, these simulations avoid complications associated with
 128 time-evolving forcings, event-to-event ENSO variability, and background SST biases. On the other hand, while perpetual,
 129 ENSO conditions help isolate atmospheric responses, they also preclude direct comparison with observation-based datasets,
 130 which include event-to-event variability, for example. The perpetual-ENSO experiments used here are a continuation of the
 131 QBOi Phase 1 experiments and have companion studies that examine ENSO’s effect on the QBO (Kawatani et al., 2025) and
 132 the combined influence of ENSO and the QBO on global teleconnections (Naoe et al., 2025).

133 2 Methods

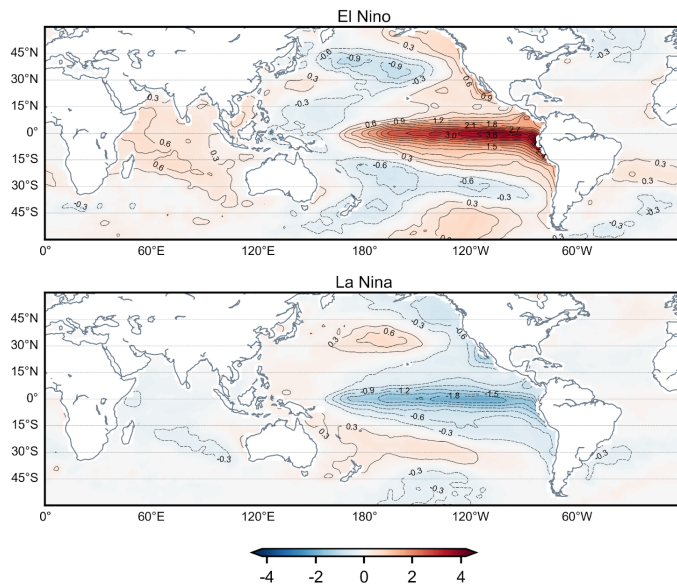
134 2.1 Experimental setup

135 Butchart et al. (2018) established a set of simplified modeling experiments for Phase 1 of the QBOi. Their Experiment 2, the
 136 “present-day time slice” simulation, forms the basis for these perpetual ENSO simulations. It was designed to allow for an
 137 evaluation of the accuracy of modeled QBOs under present-day conditions, that is, how the model QBOs operate in a climate
 138 forced with fixed repeating annual cycles of global sea surface temperature (SSTs), sea ice concentration (SIC), and external
 139 forcings representative of the time averaged 1988-2007 state.

141 The perpetual ENSO runs analyzed here are equivalent to Experiment 2, but with global El Niño or La Niña SST anomalies
 142 superimposed on top of the climatological SST forcing. An assessment of the MJO is not conducted for Experiment 2 because
 143 essential variables such as daily horizontal winds, outgoing longwave radiation (OLR), and precipitation, were not archived.
 144 In creating the composite El Niño or La Niña forcings, the characterization of ENSO follows the Japan Meteorological Agency
 145 (JMA) convention, where ENSO is defined by the spatially averaged NINO.3 (5°S-5°N, 150°W-90°W) monthly SST anomalies
 146 from 1950-2016. Anomalies are defined as deviations from the climatological seasonal cycle and computed relative to the
 147 most recent sliding 30-year period of JMA COBE-SST version 1 data (JMA, 2006). The anomalies are smoothed using a five-
 148 month running mean and the periods during which the anomalies exceed 0.5°C (-0.5°C) for at least six consecutive months
 149 are labeled as El Niño (La Niña) periods. However, after averaging the SST anomalies for all El Niño Januarys, Februarys,

- Formatted: Header
- Deleted: which may also
- Formatted: Font color: Text 1
- Deleted: While previous work has explored aspects of these interactions, we
- Formatted: Font color: Auto
- Deleted: them using
- Formatted: Font color: Auto
- Deleted: coordinated protocol
- Formatted: Font color: Auto
- Deleted: -
- Formatted: Font color: Auto
- Formatted: Font color: Text 1
- Deleted: .
- Formatted: Font color: Text 1
- Deleted: (CMIP, AMIP)
- Deleted: such
- Formatted: Font color: Text 1
- Formatted: Font color: Text 1
- Deleted: Although these simulations are well suited to detect
- Formatted: Font color: Auto
- Deleted: -driven
- Deleted: are limited in their real-world applicability, and so we ...
- Deleted: analyze Phase 1 QBOi experiments that run
- Deleted: AMIP conditions and hence, more typical ENSO amplitudes (Butchart et al. 2018, Experiments 1).
- Formatted: Font color: Auto
- Formatted: Font color: Auto
- Formatted: Font color: Auto
- Formatted: Font color: Text 1
- Deleted: in preparation
- Deleted: in preparation

168 etc., and doing the same for La Niña, the composite average annual cycles of El Niño and La Niña SSTs show only modest
 169 amplitudes (e.g., 1.92 °C for El Niño Januarys). To amplify the atmospheric response to ENSO in the simulations [and increase](#)
 170 [the signal-to-noise ratio](#), the annual cycles are multiplied by 1.8 and 1.4, respectively, making their amplitudes comparable to
 171 the strongest observed ENSO events. A similar scaling is applied to the corresponding global signatures in NINO.3 SST
 172 anomalies (Fig. 1), which are superimposed on 1988–2007 climatological SSTs and prescribed in the models. Note that this
 173 procedure does not completely capture the development, mature phase, and decay of all observed El Niño events, due to
 174 diversity in the evolutions of events. [We refer the reader to Kawatani et al. \(2025\) for more details on the experimental design](#)
 175 [and sensitivity of the model QBOs](#).



176
 177 **Figure 1: November-April composites of the El Niño (top) and La Niña (bottom) JMA COBE SST anomalies (units K) that are**
 178 **prescribed in the perpetual ENSO simulations.**

179 In addition to the prominent El Niño and La Niña signals, the November-April (NDJFMA) SSTs shown in Figure 1 include
 180 the signatures of the basin-scale Interdecadal Pacific Oscillation (IPO) (Henley et al. 2015) and Indian Ocean SSTs that are in
 181 phase with ENSO. In some regions like the tropical Pacific and Indian Oceans, the amplitude of the global SSTs associated
 182 with the El Niño are roughly double that of La Niña (Fig. 1).

184 2.2 Models

Formatted: Font color: Text 1

Deleted: (Fig. 1b)

Deleted: 1a

187
188 **Table 1:** The models used in this study, the *horizontal (given as spectral triangular truncation, T, or longitude-latitude increments) and*
189 *vertical configuration (number of levels and model top, in hPa), the number of years per simulation, and relevant literature for the convective*
190 *schemes. Only one realization is used from each model.*

Model	Horizontal resolution	Vertical levels (top, hPa)	Number of years	Convective parameterizations
EC-EARTH3.3	T255	91 (0.01)	101	Bechtold (2014)
ECHAM5sh	T63	95 (0.01)	40	Tiedtke (1989), Nordeng (1994)
EMAC	T42	90 (0.01)	106	Tiedtke (1989)
LMDz6	2°-1.25°	79 (0.015)	80	Emanuel (1991), Hourdin et al. (2013)
GISS-E2-2-G	2°-2.5°	102 (0.002)	30	Rind et al. (2020); Kelley et al. (2020)
MIROC-AGCM-LL	T106	72 (1.2)	100	Pan and Randall (1998); Emori et al. (2001)
MIROC-ESM	T42	80 (0.0036)	100	Pan and Randall (1998); Emori et al. (2001)
MRI-ESM2.0	T159	80 (0.01)	50	Yukimoto et al. (2019)
CESM1(WACCM5-110L)	1.25°-0.94°	110 (6.1E-6)	101	Zhang and McFarlane (1995)

191 The models considered are listed in Table 1 along with the number of years analyzed for each model and references on each
192 model's convective parameterization. These parameterizations impact the representation of tropical phenomena (Holt et al.
193 2020; Kawatani et al., 2025), including the simulation of intraseasonal oscillations (Ham and Hong, 2013). For example, past
194 sensitivity tests with the version of MIROC-ESM that we use here have shown that its cumulus parameterization struggles to
195 simulate an MJO of realistic amplitude with capability to propagate over the Maritime Continent (Miura et al. 2012). The
196 updated scheme (Chikira and Sugiyama 2010) in use in newer versions of the model, MIROC6, has helped ameliorate these
197

- Formatted [1]
- Commented [FS1]: I've changed the vertical column [2]
- Deleted: some ...elevant literature. [3]
- Formatted Table [4]
- Formatted [5]
- Formatted [6]
- Formatted [7]
- Formatted [8]
- Deleted: levels up to [9]
- Formatted [9]
- Deleted: hPa [10]
- Formatted [10]
- Deleted: levels up to [11]
- Deleted: hPa [12]
- Formatted [12]
- Formatted [13]
- Formatted [14]
- Formatted [15]
- Formatted [16]
- Deleted: levels up to [17]
- Formatted [17]
- Deleted: hPa [18]
- Formatted [18]
- Deleted: levels up to [19]
- Deleted: hPa [19]
- Formatted [19]
- Formatted [20]
- Formatted [21]
- Formatted [22]
- Deleted: levels up to [23]
- Deleted: hPa [23]
- Formatted [23]
- Formatted [24]
- Formatted [25]
- Formatted [26]
- Deleted: levels up to [27]
- Deleted: hPa [27]
- Formatted [27]
- Formatted [28]
- Formatted [29]
- Formatted [30]
- Deleted: levels up to [31]
- Formatted [31]
- Formatted [32]
- Formatted [33]
- Deleted: hPa [34]
- Formatted [34]
- Deleted: levels up to [35]
- Deleted: hPa [35]
- Formatted [35]
- Formatted [36]

245 issues (Ahn et al. 2017; 2020). The importance of simulated convection-circulation coupling has been identified for other
246 models (Kim et al. 2014; Zhu et al. 2020; Wang et al. 2022).

247 2.3 Observation-based reference data

248 To be consistent with previous studies (e.g., Wei and Ren 2019), the ENSO-MJO relationship is considered during
249 November-April. The six historical La Niña years, where the year is associated with November, are 1970, 1984, 1988, 2017,
250 2020, and 2021 and the eight El Niño years are 1968, 1982, 1986, 1991, 1997, 2009, 2015, 2018. Each corresponds to an
251 instance when the smoothed Niño3 anomalies exceed $\pm 0.5^{\circ}\text{C}$ for at least six consecutive months. For comparison with the
252 models, the subsequent analyses include “observed” El Niño and La Niña composites, formed by averaged deseasonalized
253 1959-2022 ERA5 reanalysis (Hersbach et al. 2020) over the years. Unlike the model simulations, which prescribe ENSO
254 SST anomalies scaled by factors of 1.8 (El Niño) and 1.4 (La Niña), the ERA5 composites reflect unscaled, event-based
255 variability. While this distinction makes direct comparison between models and reanalysis imperfect, ERA5 nonetheless
256 provides a useful benchmark for expected atmospheric responses. The ERA5 El Niño and La Niña composites are best
257 interpreted in relation to each other, rather than as strict analogs to the simulations.

258 Satellite-based daily precipitation estimates from a 1996-2023 Global Precipitation Climatology Project (GPCP, v1.3) record
259 (Huffman et al. 2001; Adler et al. 2017) are used to assess ENSO-related precipitation anomalies, as is NOAA Interpolated
260 Outgoing Longwave Radiation (Liebmann and Smith 1996). For these analyses, El Niño and La Niña years are defined as
261 ± 1 variations in standardized November-April Niño3 anomalies, yielding 1997, 2009, and 2015, and La Niña years as
262 1999, 2007, and 2010. Unlike ERA5, where cloud fields and precipitation are parameterized without direct assimilation,
263 satellite-based datasets provide a more direct observational reference, particularly valuable in the tropics where reanalysis
264 precipitation is known to be less reliable (Gehne et al. 2016).

265 2.4 MJO analyses

266 We implement a number of widely-used methods to evaluate the MJO in the perpetual ENSO simulations. In the interest of
267 exploring changes to MJO lifetime by ENSO phase as well as visualizing the MJO’s vertical structure, we compute Real-time
268 Multivariate MJO indices (RMMs) for each perpetual ENSO simulation using the same methodology as Wheeler and Hendon
269 (2004, WH04). The RMMs are derived from a combined empirical orthogonal function (EOF) analysis of tropically averaged
270 (15°S - 15°N) anomalous daily outgoing longwave radiation (OLR), 200-hPa zonal wind (U200), and 850-hPa zonal wind
271 (U850). As in WH04, we deseasonalize, remove interannual variability, and normalize the anomalies by their global variance.
272 To enable a fairer comparison between the models and reanalysis, we project the anomalous model fields onto the 1959-2022
273 ERA5 WH04 EOFs; projecting onto each model’s respective ENSO simulation instead does not change the conclusions. Daily

Formatted: Header

Formatted: Font color: Text 1

Formatted: Font color: Text 1

Formatted: Left, Space Before: 12 pt, After: 12 pt

Deleted: to

Deleted: observed

Formatted: Font color: Text 1

Formatted: Font color: Text 1

Deleted: NINO.3

Deleted: 5C

Formatted: Font color: Text 1

Formatted: Font color: Text 1

Deleted: averaging

Formatted: Font color: Text 1

Deleted: aforementioned

Deleted: These El Niño and La Niña composites are not

Formatted: Font color: Text 1

Deleted: , respectively, in contrast to the ENSO SSTs prescribed in the simulations. Hence

Deleted: responses are

Formatted: Font color: Text 1

Deleted: be more modest in amplitude compared with responses from the models. However, the difficulties that the models have simulating the MJO in some respects can render this untrue in practice

Formatted: Font color: Text 1

Formatted: Font color: Text 1

Formatted: Underline, Font color: Custom Color(RGB(0,120,212))

Formatted: Font color: Text 1

Formatted: Font color: Text 1

290 OLR and U200 were not available for two models (GISS-E2-2-G and LMDz6) so their RMMs are computed using U250 and
291 U850.

293 The number of MJO events within a given data set is tallied like in Pohl and Matthews (2007) by counting the number of times
294 the MJO makes a complete rotation through its RMM1 and RMM2 phase space. Average lifetime and MJO amplitudes
295 $\sqrt{(RMM1^2) + (RMM2^2)}$ are computed across events. To visualize the MJO's vertical structure, latitudinally averaged
296 10°S-10°N longitude-pressure cross-section of zonal wind and temperature are projected onto the RMMs using the same steps
297 as Hendon and Abhik (2018), but applied across ENSO years in the present study rather than QBO years.

299 The MJO is visualized using two related wavenumber-frequency approaches. Both Fourier transform deseasonalized and
300 detrended, highpass filtered, tapered time-longitude data, reorder coefficients into eastward/westward components, and
301 compute power spectra to isolate intraseasonal variability. The CLIVAR MJO metric (Waliser et al., 2009) applies this to
302 centered November-April segments of tropical U850, yielding single variable power for eastward and westward disturbances
303 (Figure 3). The Wheeler and Kiladis (1999) style analysis is similar, but designed to diagnose the broader family of
304 convectively coupled equatorial waves alongside the MJO; we linearly detrend multiyear daily fields, highpass filter at 96 days,
305 use overlapping 96-day segments (65-day overlap), perform successive longitude-time transforms, recover symmetric and
306 antisymmetric spectra about the equator, and normalize by a smoothed background; results are presented as the ratio of raw
307 symmetric daily mean precipitation power to background (Figure 2). To sharpen the MJO and facilitate comparison with the
308 CLIVAR metric, our Wheeler-Kiladis implementation also subsets data to November-April. For model evaluation, spectra are
309 divided by each model's perpetual ENSO background, whereas GPCP (ERA5) El Niño and La Niña spectra are compared to
310 a common 1996-2022 (1959-2022) background; GPCP and ERA5 conclusions are insensitive to using regime specific
311 backgrounds.

313 We also implement an MJO diversity analysis in which MJO events are classified into distinct types based on their propagation
314 characteristics using k-means clustering (Wang et al. 2019). Each MJO event is binned as one of four archetypes, "standing"
315 or "jumping" MJOs, which propagate across the Indian Ocean, but are distinguished by reemergence of the MJO over the
316 western Pacific during jumping events, and "slow" or "fast" MJOs, which both continuously propagate across the Maritime
317 Continent, but at different speeds. An MJO event occurs when the 20-70 day bandpass-filtered OLR anomalies (from seasonal
318 cycle) averaged over the equatorial Indian Ocean (10°S-10°N, 75°E-95°E) are smaller than negative one standard deviation
319 for five successive days; the reference day (day 0) is the day of minimum OLR. The MJO events are categorized by a k-means
320 clustering of the enhanced convective signal (OLR anomalies under -5 Wm^{-2}) of the latitudinally averaged 10°S to 10°N time-
321 longitude OLR anomalies taken over 60°E to 180°E and over a 31-day period from day -10 to day 20. For brevity, we omit
322 further diversity analysis methodological details, for which we refer the reader to Back et al. (2024) for all steps. Unlike Wang
323 et al. (2019), in which initial centroids for clustering are randomly chosen, initial centroids for model MJO events are set to

Formatted: Header

Commented [FS2]: something's wrong with this formula. I suggest using something like "summed in quadrature" or similar

Commented [FS3R2]: mm, the change in formula can't be tracked

Deleted: $(\sqrt{RMM1^2 + RMM2^2})$

Deleted: also ...visualized using two slightly different ...related wavenumber-...frequency filtering analyses. The first, available via the MJO US Climate Variability...pproaches. Both Fourier transform deseasonalized and Predictability (...trending, highpass filtered, tapered time-longitude data, reorder coefficients into eastward/westward components, and compute power spectra to isolate intraseasonal variability. The CLIVAR) metrics package...MJO metric (Waliser ...et ...al. ...2009), is computed by Fourier transforming in time and longitude deseasonalized, tapered, and ... [43]

Commented [FS4]: We might mention that this choice may artificially introduce power around 180 days

Commented [de5R4]: True. I added this, but put it in the caption beneath Figure 3

Deleted: OLR and ...850, reorganizing the Fourier coefficients ...ielding single variable power for eastward and westward disturbances (Hayashi 1982) and computing power, Figures ...figure 3 and 4 respectively..... The second filtering technique is broadly ...heeler and Kiladis (1999) style analysis is similar, but specializes in resolving designed to diagnose the broader family of convectively coupled equatorial waves in addition to ...longside the MJO (Wheeler and Kiladis 1999). Prior to this analysis, the multi-year... we linearly detrend multiyear daily-mean...fields ERA5 and each model are linearly detrended, high pass filtered for intraseasonal variability using a... highpass filter 96-day cutoff, grouped into ...days, use overlapping 96-day segments that share ...65 days of...day overlap with neighboring segments, and each segment is linearly detrended and tapered. Successive discrete Fourier..., successive longitude-time transforms are applied in longitude and time, the coefficients are reordered (Hayashi 1982), we retrieve the ... recover symmetric and antisymmetric components of a given field's ...pectra with respect to...bout the equator, and then divide each component...ormalize by a smoothed background spectrum. The resulting power spectrum, shown... results are presented as the ratio between...f raw symmetric daily-...mean precipitation power and the...o background spectrum in 2, reveals the modes of organized convection with the most power. Model...Figure 2). To sharpen the MJO and facilitate comparison with the CLIVAR metric, our Wheeler-Kiladis implementation also subsets data to November-April... [44]

Deleted: However, it is important to note that unlike

494 those of the four observation-based clusters, allowing the present study to evaluate how well climate models reproduce
495 observed MJO diversity with minimal subjectivity.

496 2.5 QBO and analyses

497 The space-time form of the QBOs varies from model to model as each is generated with different amounts of forcing from
498 resolved waves and parameterized non-orographic gravity wave drag. Properties of these models that are particularly relevant
499 for simulating the QBOs are listed in Butchart et al. (2018), details on QBO morphology (e.g., its amplitude, latitudinal width)
500 given the observed SST record are presented in Bushell et al. (2022), and the relative contribution of resolved and
501 parameterized tropical waves to forcing the QBO is analyzed in detail in Holt et al. (2020). Of note, MIROC-AGCM-LL's
502 QBO is forced solely by resolved waves. As EC-EARTH and GISS-E2-2-G did not contribute to some of the earliest QBOi
503 analyses, relevant details on their internal QBOs can be found in Serva et al. (2024) and Rind et al. (2014, 2020), respectively.
504 For a thorough analysis of how the QBO responds to the perpetual ENSO simulations, we refer the reader to Kawatani et al.
505 (2025).

506
507 To help clarify the ability of the QBOs to interact with the MJOs, we use established metrics to characterize the morphology
508 of the ERA5 and model QBOs. The main field used to document QBO morphology is the monthly zonal-mean zonal wind.
509 "QBO cycles" (consecutive easterly/westerly phases) are identified by marking the first month when the deseasonalized and
510 smoothed (5-month running mean) 20 hPa 5°S-5°N wind changes from westerly to easterly, ending one month before the next
511 transition at 20 hPa (Kawatani et al. 2019). From these cycles, we calculate average QBO easterly, westerly, and total
512 amplitudes using the QBO "transition time" methodology of Richter et al. (2020). The easterly (westerly) amplitude is equal
513 to the average of the minimum (maximum) monthly QBO winds from each QBO cycle. The QBO cycles are used further to
514 calculate minimum, mean, and maximum QBO periodicity statistics. These statistics are a key result of Kawatani et al. (2025)
515 and are discussed thoroughly there. In short, the periodicity of the QBO decreases in all El Niño simulations and increases in
516 all La Niña simulations, which is attributed to ENSO modulating convection and the low-frequency circulation, thereby
517 influencing generation of tropical waves and their filtering by the large-scale circulation and the QBO. For the purposes of the
518 present study, the minimum and maximum periodicities are required to evaluate the QBO's spatial structure, defined as the
519 latitude-pressure cross sections of each data set's QBO Fourier amplitude. These are made by applying a discrete Fourier
520 transform in time to the multi-year monthly zonal-mean zonal wind at each pressure-latitude grid point and dividing the sum
521 of squares of the amplitudes of the harmonics corresponding to periods between the minimum and maximum QBO periods by
522 the sum of squares of the amplitudes of all harmonics. This ratio is subsequently multiplied by the standard deviation of the
523 zonal-mean zonal wind (Pascoe et al. 2005). Using this QBO Fourier amplitude, the lowest altitude the QBO reaches, its
524 vertical extent (i.e., how tall it is), and its latitudinal extent are defined as in Schenzinger et al. (2017), except that here the
525 QBO's maximum amplitude is assumed to be at 20 hPa for all models and ERA5.

Formatted: Header

Deleted: to minimize subjective decisions. Because of this step, herein...

Deleted: evaluates

Deleted: the

Deleted: can

Deleted: the

Deleted: archetypes

Deleted: EG

Deleted: (in preparation)

Deleted: (in preparation)

Deleted: .

537

538 ~~QBO impact on~~ the MJO is assessed using the techniques of Klotzbach et al. (2019) and Kim et al. (2020). Following the prior,
 539 we make scatterplots of December-February warm-pool (10°S-10°N, 45°E-180°E) averaged tropopause stability (100 hPa
 540 minus 200 hPa temperature) versus December-February MJO amplitude as a function of QBO phase (sign of DJF averaged
 541 5°S-5°N 50 hPa zonal mean zonal-wind) for each of the simulations. MJO amplitude is expected to increase as tropopause
 542 stability decreases, which happens during the easterly QBO phase. As in Kim et al. (2020), MJO activity is also computed as
 543 a function of QBO phase. Specifically, MJO-filtered OLR is calculated following Wheeler and Kiladis (1999) with one
 544 exception, the full time series is detrended rather than using 96-day overlapping segments. To minimize spectral leakage, 5%
 545 of the data are tapered to zero at the ends of the timeseries. After tapering, a complex Fourier Transform is performed, and the
 546 spectral wavenumber-frequency data are filtered to retain only the eastward propagating coefficients for 20-100 day periods
 547 and wavenumbers 1-5. MJO activity is then defined as the standard deviation of the MJO-filtered OLR across all December-
 548 February days that fall into a particular category, for instance all years, easterly QBO years or westerly QBO years. For this
 549 analysis, easterly and westerly QBO years are defined as those which exceed +/- 0.5 standard deviation of the 50 hPa monthly
 550 zonal wind anomalies, seasonally smoothed and averaged over 10°S to 10°N. ~~We allow the QBO to be defined differently~~
 551 between the Klotzbach and Kim et al. ~~Analyses; herewe prioritize~~ using the aforementioned metrics in their original form
 552 rather than using ~~customizing them~~.

553

3 Results

554

3.1 ENSO-MJO interaction

555 Before examining the influence of ENSO on MJO, we evaluate some of the other large-scale tropical phenomena that the
 556 models simulate. Convectively coupled waves are relevant because they comprise the space-time structure of the MJO and can
 557 influence its propagation by modulating the tropical circulation and the distribution of moisture that the MJO encounters
 558 (Kiladis et al. 2009; Wang et al. 2019; Wei and Ren 2019; Berrington et al. 2022; Wang and Li 2022). Aspects of the waves,
 559 such as their phase speed, vary depending on the low frequency circulation (Roundy 2012). Hence, the amplification of the
 560 Walker Circulation by La Niña and the weakening of it by El Niño (Fig. S1) provide a pathway for the perpetual ENSO
 561 forcings to modulate the waves and perhaps the MJO. Applying similar methods to Wheeler and Kiladis (1999), we visualize
 562 the waves by computing the spectral power of ERA5 and model daily-averaged precipitation as a function of wavenumber and
 563 frequency. Figure 2 shows the precipitation spectra for phenomena symmetric about the equator, taken over November-April
 564 and 15°S-15°N. Three dispersion curves, as in Matsuno (1966), corresponding to equivalent depths of 10, 25, and 50 meters
 565 are also superimposed; these curves are derived using the dispersion relations for equatorially trapped waves and they are co-
 566 located with modes of organized convection, with larger equivalent depths corresponding to faster phase speeds.

567

Formatted: Header

Deleted: The QBO's capability to

Deleted: the tropical tropopause and

Deleted: further

Deleted: One may notice that

Deleted: is

Deleted: analyses. Herein, we have prioritized

Deleted: customized metrics so as to have one uniform definition of, for instance, QBO phase

Deleted: coupling

577 [The GPCP panels in row one draw on only three La Niña and three El Niño years, while the ERA5 panels in row two use just](#)
578 [six La Niña and eight El Niño years, resulting in signals that are noisier than the models' multi-decade averages. Power is](#)
579 [typically the highest amplitude in GPCP, then ERA5, and weakest in](#) the models. Spectral signals associated with the eastward
580 propagating Kelvin wave move up and to the right on each panel, spanning sub-planetary low frequency ($\sim k = 3, 25$ days)
581 scales to synoptic ($k = 4+$) sub-weekly scales. Relative to [GPCP and ERA5](#), the models underestimate the strength of the
582 Kelvin wave, [irrespective of the type of ENSO forcing, but have worse difficulties in the El Niño simulation](#). Power associated
583 with the westward propagating equatorial Rossby wave is evident on the left side of each panel between wavenumbers 1-10
584 and timescales of 10 days to five weeks. Overall, the models do a reasonable job of simulating the spectral amplitude of
585 equatorial Rossby waves, although it is too strong for some models (EMAC, MIROC-ESM), especially in their La Niña
586 simulations.
587

Formatted: Header

Deleted: Only

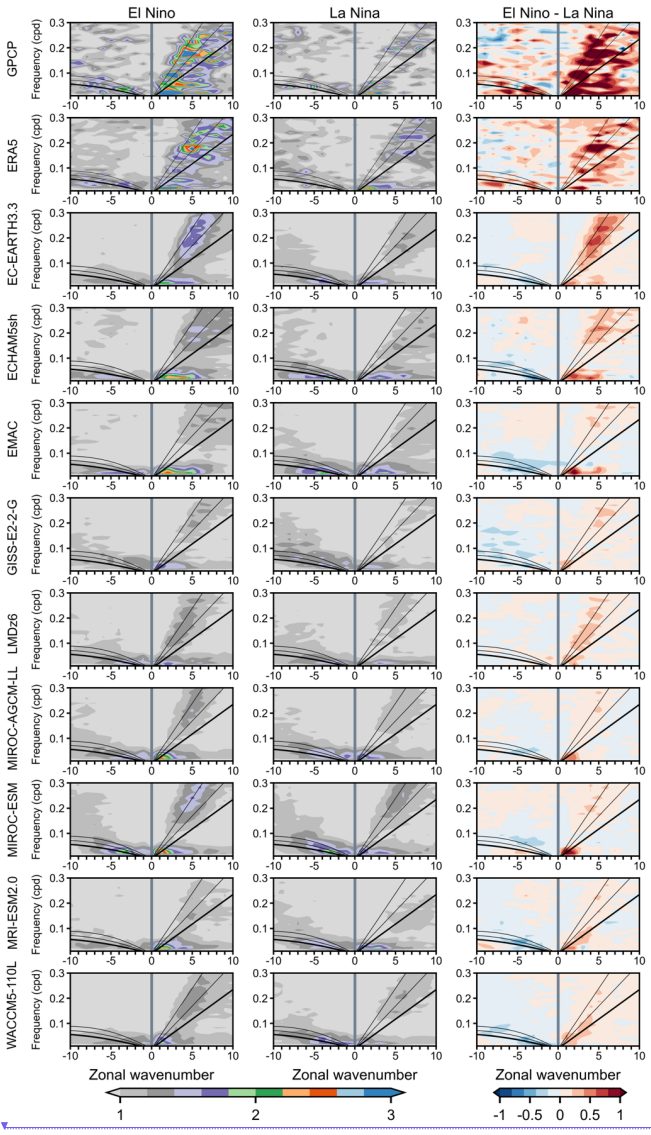
Deleted:

Deleted: Niño events are used to make the ERA5 equivalent figures that are shown in row one, which coincides with these...

Deleted: being noisy compared to

Deleted: from

Deleted: and this happens



Formatted: Header

Deleted: <object>

598 **Figure 2: Wavenumber-frequency spectrum of the symmetric component of 15°S-15°N November-April precipitation plotted as the**
599 **ratio between raw symmetric precipitation and a smoothed red noise background spectrum. The eastward (right) side of the**
600 **spectrum includes three Kelvin wave dispersion curves in black, of which the thickest curve corresponds to the equivalent depth of**
601 **12 meters, and the others to 25 and 50 meters, respectively. Similar dispersion curve plotting conventions are used on the westward**
602 **(left) side of the spectrum where the curves overlay the equatorial Rossby wave power. Column one corresponds to El Niño, column**
603 **two to La Niña, and column three to their difference, which is computed as (El Niño symmetric minus El Niño background) minus**
604 **(La Niña symmetric minus La Niña background). Computing the third column as (El Niño symmetric) minus (La Niña symmetric)**
605 **yields similar conclusions (not shown).**
606

607 The effect of ENSO phase on each wave is revealed by the rightmost column of Figure 2, which shows El Niño (column one)
608 minus La Niña (column two) differences, where red means stronger power during El Niño and blue means larger power during
609 La Niña. All models simulate stronger Kelvin waves in their El Niño simulation, particularly along the deeper equivalent depth
610 ($n = 25, 50$ meters) dispersion curves. This implies faster Kelvin wave phase speeds during El Niño. Examining the El Niño
611 column, the alignment of the Kelvin wave power along these particular curves is demonstrated by EC-EARTH3.3, GISS-E2-
612 2-G, LMDz6, MIROC-AGCM-LL, MIROC-ESM, MRI-ESM2.0 and (CESM1) WACCM5-110L, hereafter just “WACCM5-
613 110L.” The remaining models, ECHAM5sh and EMAC (both ECHAM-based models), differ in that their El Niño Kelvin wave
614 power is weighted towards higher zonal wavenumbers for frequencies below 0.2 cpd. Similar to the models, GPCP and ERA5
615 shows large sporadic increases in Kelvin wave power along deeper equivalent depth dispersion curves during El Niño
616 compared to La Niña. In contrast, for the westward propagating equatorial Rossby wave, GPCP and ERA5 indicate stronger
617 power during El Niño, whereas all models simulate stronger Rossby wave power during La Niña. This discontinuity arises
618 from models underestimating average equatorial Rossby wave spectral power during El Niño, while overestimating power
619 during La Niña, relative to GPCP and ERA5 (not shown).
620

621 Having found changes in the convectively coupled waves due to ENSO, perhaps the model MJOs also behave differently given
622 ENSO state. Broadly speaking, Figure 2 shows that the models include MJOs as indicated by the maxima in spectral power at
623 intraseasonal timescales ($\ll 0.1$ cpd) between eastward propagating wavenumbers 1-5. Holt et al. (2020) also found MJOs to
624 be simulated by these models in historical AMIP simulations (QBOi Exp 1). The highest MJO power in GPCP is concentrated
625 between wavenumbers 1 and 3 and exceeds that of ERA5 and the models. EC-EARTH3.3, MIROC-AGCM-LL, MIROC-
626 ESM, MRI-ESM2.0 correctly position MJO power between wavenumbers 1-3 whereas ECHAM5sh, EMAC, (sharing
627 convective parameterizations) and LMDz6 exhibit spectral power that is incorrectly shifted towards higher wavenumbers. The
628 amplitude of the MJO is comparatively small in GISS-E2-2-G, LMDz6, and WACCM5-110L, which may adversely affect
629 their stratospheric waves, since these three models adopted interactive GW sources. The El Niño minus La Niña differences
630 in the rightmost column of Figure 2 show that MJO spectral power is stronger in the presence of the El Niño basic state.
631 Differing from the other models, EC-EARTH3.3, ECHAM5sh, and EMAC have fairly large El Niño minus La Niña MJO
632 power differences at wavenumber 4 and 5.
633

Formatted: Header

Commented [FS6]: there is something strange with Figure 2...are there two images overlapped?

Commented [FS7R6]: the one in background seems to have lower resolution

Commented [de8R6]: Yes, the old Figure was in the background - i deleted it

Deleted: power

Deleted: power

Deleted: other two correspond

Deleted: E

Deleted: Agreement between ERA5 and the models is less clear when instead considering

Deleted: . All

Deleted: . There is a tendency in some models for this

Deleted: happen along the deeper equivalent depth dispersion curves (e.g., MIROC-AGCM-LL, MIROC-ESM).

Deleted: are

Deleted: modulated by

Deleted: do in fact

Deleted: .

Deleted: ERA5

Deleted: irrespective

Deleted: ENSO phase.

Deleted: are closest to reproducing this

Deleted: .

Commented [FS9]: to check: may cite this one DOI 10.1007/s00382-012-1343-y for LMDz poor MJO

Commented [FS10R9]: maybe not to cite, but I found a few MJO works where LMDz is nudged...<https://agupubs.onlinelibrary.wiley.com/doi/full/10.1002/2015JD023461> we could mention MJO/QBO nudging in Discussion section?

Commented [de11R9]: Omitting this for brevity

Deleted: shown

Deleted: highlight

Deleted: . predominantly between wavenumbers 2 and 3 in ERA5 and wavenumbers 1 and 2 across the majority of the models....

658 Irrespective of ENSO phase, the amplitude of the model MJOs as shown in Fig. 2 is systematically weaker than in [GPCP](#) or
659 ERA5. This may have something to do with dividing each simulation's symmetric power by its respective background power,
660 the latter of which is contaminated, in a sense, by the perpetual ENSO conditions. Note that recomputing the third column of
661 Fig. 2 without dividing each El Niño and La Niña composite by their respective background does not change our conclusions
662 (not shown). To get around this potential issue with the background power and further inspect the model MJOs as opposed to
663 the convectively coupled waves, in Figures 3 we consider the westward and eastward wavenumber-frequency spectra of
664 [U850taken](#) over the intraseasonal timescale and over MJO-like zonal wavenumber scales. These analyses yield more holistic
665 views of the MJO than in Fig. 2 because they incorporate the MJO's signals in these fields that are both symmetric and
666 antisymmetric about the equator.

Formatted: Header

Deleted: and 4

Deleted: OLR and U850, respectively, taken

Formatted: Centered

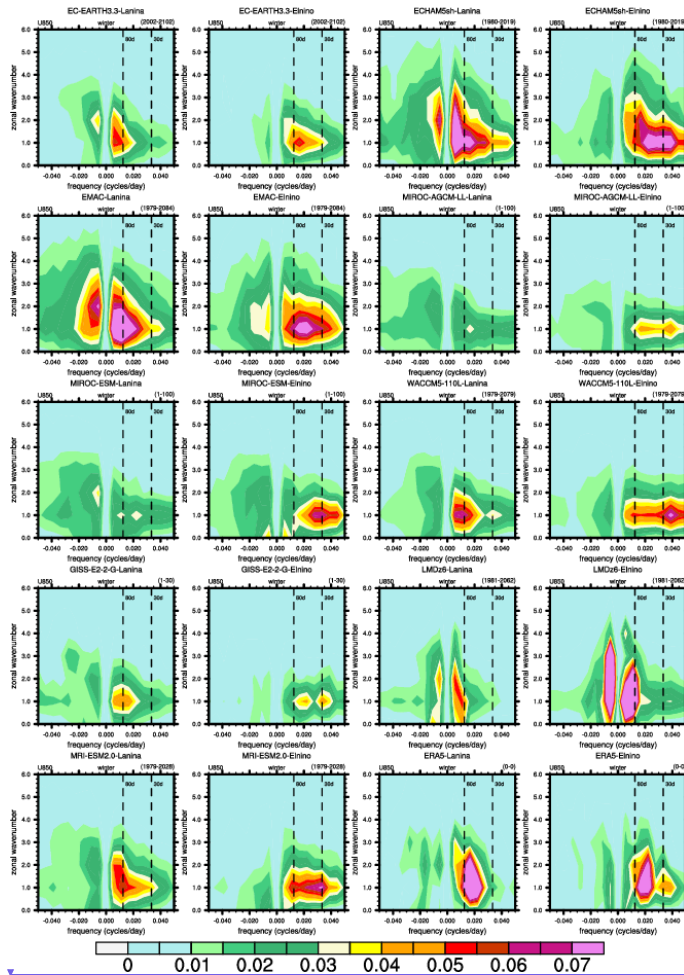
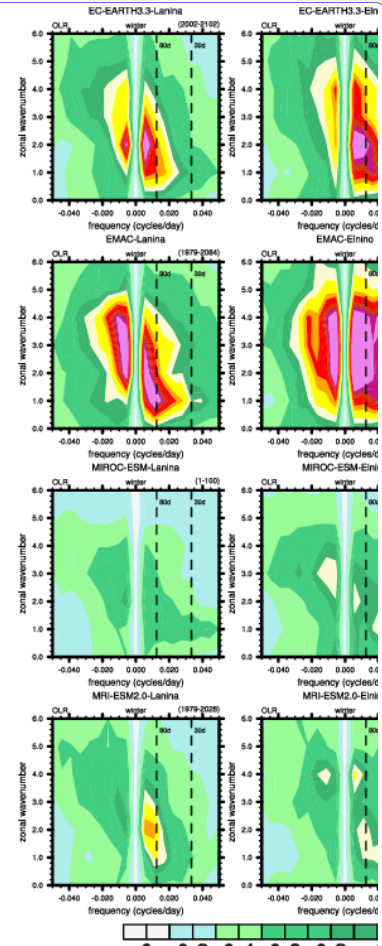


Figure 3: November-April wavenumber-frequency power spectra of 10°S - 10°N averaged U_{850} . Units of the U_{850} spectrum are m^2/s^2 per frequency interval per wavenumber interval. We interpret the power at ~ 180 -day frequencies as a by-product of using centered November-April segments.

As shown by ERA5, the MJO timescale variance of dynamical fields such as U_{850} are known to have a narrow spectral peak around zonal wavenumber 1 (Hendon and Salby 1994). The models are fairly good at reproducing this (Fig. 3), despite large

Formatted: Header



Deleted:

Deleted: OLR...850. Units of the OLR...850 spectrum are W^2/m^4 ... [45]

Deleted: Observed...s shown by ERA5, the MJO timescale variance associated with convective...f dynamical fields like OLR predominantly spans...uch as U_{850} are known to have narrow spectral peak around zonal wavenumber ...1-3 and frequencies corresponding to periodicities of 1-3 mor... [46]

inter-model differences in terms of peak amplitudes. Independent of the ENSO phase, ERA5's wavenumber-frequency shows the highest power between frequencies of 30-80 days (vertical dashes), a so-called "MJO band" (Ahn et al. 2017). Considering only the ERA5 MJO band, the MJO is stronger given lower zonal wavenumbers and longer periodicities during La Niña compared to El Niño. Similarly, the model spectra broadly indicates that the periodicity of the MJO decreases during El Niño and increases during La Niña. However, as was the case for the symmetric precipitation spectra (Fig. 2), there are notable differences in the amplitude of the spectral power between models and reanalysis. Of the models, MJO band amplitude in ECHAM5sh and EMAC is most like ERA5, whereas other models, particularly MIROC-AGCM-LL, MIROC-ESM, and GISS-E2-2-G significantly underestimate the strength of the MJO in this metric. Another issue is that models exhibit too large of an MJO signal for zonal wavenumbers three and up, which is unrealistic and common amongst GCMs (Ahn et al. 2017), with particularly exaggerated high-wavenumber amplitudes in ECHAM5sh, EMAC, and LMDz6, as previously noted for precipitation. The clustering of models related to each other, such as MIROC and ECHAM-based models, indicate that also the tropospheric wind response to imposed ENSO anomalies is strongly influenced by model configuration and convective schemes.

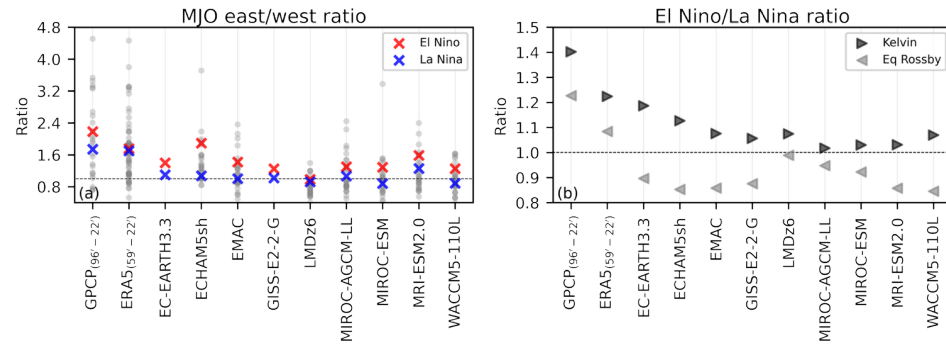
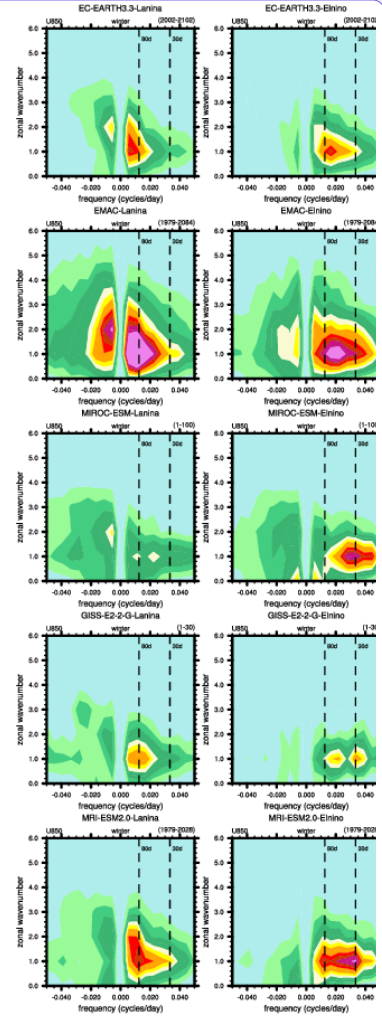


Figure 4 (a) Ratio of eastward to westward MJO precipitation spectral power (from Figure 2) filtered for wavenumbers +/- 1 to 3 and 30 to 96 day frequencies. Red and blue X's denote El Niño and La Niña, respectively, using the same notation for both the GPCP and ERA5 composite averages and the climatological values from the perpetual El Niño and La Niña simulations. Gray dots indicate interannual east/west ratios from GPCP, ERA5, and the QBOi Experiment 1 simulations (1979-2009 AMIP) by these same models; EC-EARTH3.3 and GISS-E2-2-G did not run Experiment 1. (b) Ratio of Kelvin wave and equatorial Rossby wave power in El Niño to that in La Niña. Each wave is filtered using equivalent depths of 8 to 90 meters, with wavenumbers of 1 to 14 for the Kelvin wave and -1 to -10 for the equatorial Rossby wave.

To further explore the MJO timescale changes suggested by Figure 3, Figure 4a shows the ratio of eastward to westward MJO spectral power in symmetric precipitation from GPCP, ERA5, and the models. The E/W ratio measures how robust MJO eastward propagation is (Jiang et al. 2015; Ahn et al. 2017). El Niño and La Niña responses in GPCP and ERA5 (red and blue X's) are derived from composites of previously defined strong ENSO seasons, while gray dots represent interannual E/W

Formatted: Header

Deleted: wavenumbers 1-3 and...frequencies of 30-80 days (vertical dashes), a so-called "MJO band" (Ahn et al. 2017). Considering only the ERA5 MJO band, the MJO is stronger given lower zonal wavenumbers and longer periodicities... [47]



Deleted: 0 0.01 0.02 ... [48]

Commented [FS12]: @Dillon please revise this caption!

Commented [FS13R12]: I guess we could say that tropical waves sensitivity is better reproduced than MJO by comparing these plots, right?

Commented [de14R12]: We could say that, but it's more true for some models (GISS, LMDz6), no? For ECHAM5sh (assuming its mean E/W ratio is ~ 1.5), the ENSO forcings drive a ~30% shift in ratio, whereas ECHAM5sh's ... [49]

Commented [FS15R12]: Yes, that's a good idea. I cited Laura's paper as RG waves are less well simulated than K waves.

Commented [FS16]: how come this paragraph is not track changed?

Commented [de17R16]: It was pasted in using editing mode, not reviewing mode

Deleted: various of dynamical fields

848 ratios across all years (GPCP: 1996–2022; ERA5: 1959–2022), providing a baseline of internal variability. Both data sets show
 849 modestly higher E/W ratios during El Niño than La Niña.

850
 851 While the model ENSO responses in Figure 4a are derived from climatological means of perpetual ENSO simulations, rather
 852 than event-based composites as in GPCP and ERA5, making direct comparison imperfect, the juxtaposition nonetheless reveals
 853 systematic differences in MJO behavior across observational and modeled frameworks. Model gray dots are interannual ratios
 854 from OBOi Experiment 1 AMIP 1979-2009 simulations, which contextualizes model internal variability. E/W ratios are higher
 855 in El Niño simulations, shifting towards the upper tail of the AMIP-based sampling variability. Conversely, many of La Niña
 856 E/W ratios are around one (dashed line), indicating subdued MJO propagation. The response to ENSO is relatively small in
 857 models with a weak MJO, such as GISS, LMDz6 and MIROC-AGCM-LL.

858
 859 Building on the observed ENSO-related changes in MJO propagation, Figure 4b further quantifies how convectively coupled
 860 equatorial waves, Kelvin and equatorial Rossby, respond to ENSO forcing, given their known links to MJO variability. Figure
 861 4b shows the ratio of El Niño to La Niña precipitation-based spectral power, filtered from Figure 2 for each wave type. GPCP
 862 and ERA5 composites indicate that both waves are stronger during El Niño than La Niña. Models generally reproduce stronger
 863 Kelvin waves in their El Niño simulations, however, equatorial Rossby waves are consistently stronger during La Niña, in
 864 contrast to GPCP and ERA5. This disagreement between observational products and models regarding is difficult to attribute
 865 given the differences in how spectra for each are computed and known biases in modeled precipitation spectra (Holt et al.
 866 2020, Experiment 1). It appears to stem from a combination of model equatorial Rossby waves being underestimated in the
 867 El Niño simulation and overestimated relative to GPCP and ERA5 in the La Niña simulation (not shown). Taken together,
 868 Figures 3 and 4 suggest that MJO periodicity tends to shorten during El Niño and lengthen during La Niña. The robustness of
 869 this relationship is further assessed using Pohl and Matthews (2007) MJO statistics, including MJO lifetime, summarized in
 870 Table 2.

871
 872 *Table 2: The number of MJO events, their mean lifetimes and standard errors (reported in parentheses), and their mean amplitudes given*
 873 *either perpetual El Niño or La Niña conditions in a model. An asterisk (*) next to a model name indicates that the RMMs were retrieved*
 874 *using only 250 and 850 hPa zonal wind. Different from the models, for ERA5, MJO event statistics are calculated using 8 El Niño and 6 La*
 875 *Niña winters subsampled from the entire 1959-2022 RMM record.*

	EN events (#/dec)	LN events (#/dec)	EN lifetime (days)	LN lifetime (days)	EN amplitude	LN amplitude
ERA5	25	22	38.25 (2.27)	47.07 (3.97)	1.36	1.41
EC-EARTH3.3	18.07	13.80	37.96 (1.25)	46.73 (2.01)	1.47	1.40
ECHAM5sh	26.20	15.87	28.59 (1.18)	42.94 (3.26)	1.43	1.38

Formatted: Header

Commented [FS18]: also this paragraph is new, no?

Commented [de19R18]: Yes, all new

Commented [FS20]: or inter-annual?

Commented [de21R20]: yeah I think inter-annual makes more sense

Formatted: Font color: Text 1

Formatted: Font color: Text 1

Formatted: Pattern: Clear (Background 1)

Deleted: U850 is

Deleted: to have a much narrower spectral peak around zonal wavenumber-1 (Fig.

Deleted:). The models are fairly good at reproducing this. Using U850 allows us to incorporate output from GISS-E2-2-G and LMDz6 for which OLR data is not available. Notwithstanding some of the typical model issues (e.g., amplitude differences compared to observations, and overly large power at high wavenumbers especially in ECHAM5sh, EMAC, and LMDz6), Figure 4 like Figure 3 indicates that the ...

Deleted: of the MJO decreases

Deleted: increases

Deleted: these results

Deleted: considered

Deleted: by

Deleted: the PM07

Deleted: which are tabulated

Formatted: Font: 10 pt, Not Bold

Formatted Table

EMAC	23.83	14.75	29.77 (0.88)	45.57 (1.93)	1.37	1.45
GISS-E2-2-G†	20.56	11.46	32.23 (1.87)	37.06 (3.50)	1.42	1.31
LMDz6*	11.30	9.81	37.01 (2.20)	32.47 (1.69)	1.55	1.41
MIROC-AGCM-LL	23.48	19.26	30.31 (0.78)	30.90 (1.11)	1.46	1.49
MIROC-ESM	27.77	18.15	27.96 (0.57)	29.90 (1.15)	1.38	1.34
MRI-ESM2.0	21.53	16.70	35.02 (1.39)	39.35 (1.88)	1.43	1.40
WACCM5-110L	26.00	16.87	27.13 (0.77)	36.99 (1.31)	1.40	1.49

Formatted: Header

Commented [FS22]: elsewhere it is called GISS-E2-EG...I guess this is the "right" name?

Commented [de23R22]: thanks for pointing this out. yes, that is the right name (see: <https://www.wdc-climate.de/ni/cmip6?input=CMIP6.CMIP.NASA-GISS.GISS-E2-2-G>), I found some incorrect spellings of it throughout, which I have revised

895 Based on ERA5, La Niña events are roughly nine days longer than El Niño events on average. Wei and Ren (2019) found La
 896 Niña to support both high-frequency (lifetime ~40 days) and low frequency (lifetime ~80 days) MJOs, which conceivably
 897 explains the much larger ERA5 lifetime standard errors during La Niña compared with El Niño. Strikingly, the difference in
 898 lifetime and its standard error between ENSO phases is nearly ubiquitous across the models. With the exception of LMDZ6,
 900 La Niña lifetimes are between 0.59 (MIROC-AGCM-LL) and 15.8 (EMAC) days longer than El Niño lifetimes. Models in
 901 similar families, for instance ECHAM5sh and EMAC as well as MIROC-AGCM-LL and MIROC-ESM, typically have similar
 902 magnitude differences in their Pohl and Matthews (2007) statistics between ENSO phases. All models simulate more MJO
 903 events during El Niño, which is consistent with ERA5, however the difference in the number of events between ENSO phases
 904 is generally larger in the models than in ERA5. MJO amplitude is only marginally larger during La Niña based on ERA5
 905 whereas six of the nine models have larger amplitudes during El Niño.

906
 907 Analyzing MJO diversity offers further insight into its propagation characteristics. K-means clustering of empirical OLR
 908 Hovmöller diagrams reveals four dominant archetypes: standing, jumping, slow, and fast propagating MJOs (Wang et al.
 909 2019). Associated SST composites show standing MJOs tend to coincide with La Niña, fast MJOs with El Niño, while jumping
 910 and slow events show no clear ENSO linkage (Back et al. 2024). The experimental design allows us to test whether certain
 911 archetypes become more robust under persistent ENSO forcing. Fast and slow events can occur during either ENSO phase
 912 (Yadav and Straus 2017), suggesting some sensitivity of the established archetype-ENSO associations to internal variability.
 913 Figure 5 lists the number of each archetype's events simulated by each model (at the base of each bar). Standing and jumping
 914 MJOs occur with similar frequency across ENSO phases, with four of seven models producing more standing events during
 915 La Niña and four models producing more jumping events during El Niño. results that do not indicate a consistent ENSO
 916 dependence. In contrast, slow and fast MJOs are modestly more frequent in El Niño simulations for six of seven models.

Deleted: can provide

Deleted: speed and

Deleted: .

Deleted: MJO convection tracks from

Deleted: reveal

Deleted: major MJO propagation

Deleted: propagating

Deleted: events

Deleted: Composites of the background SSTs associated with these archetypes

Deleted: be concurrent

Deleted: overlap

Deleted: and

Deleted: have

Deleted: association with either

Deleted: phase.

Deleted: setup here enables

Deleted: if in fact some of the MJO

Deleted: predominate given a background

Deleted: Note that fast

Deleted: and so there is at least

Deleted: previous results

Deleted: sampling

Deleted: (Yadav and Straus 2017). ¶

¶

... [50]

Formatted: Font: 10 pt, Not Bold

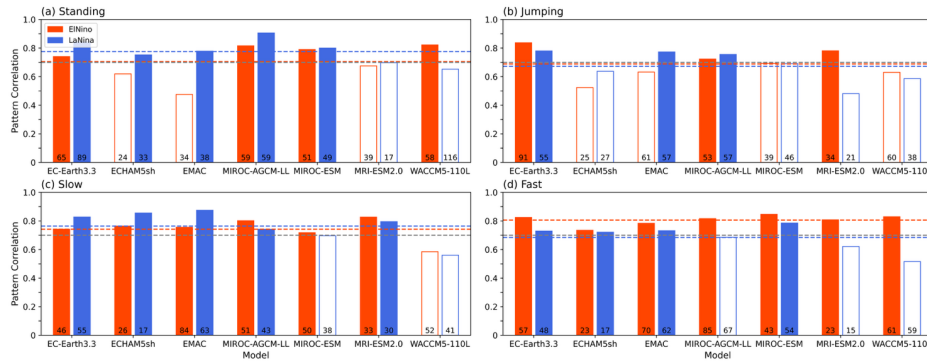


Figure 5: Pattern correlations between the ERA5 and simulated time-longitude (Hovmöller) 10°S-10°N convective OLR anomaly composites (OLR < -5 W/m²) corresponding to each of the four K-means clusters MJO archetypes defined in Wang et al. (2019). Multi-model average El Niño and La Niña correlations are shown by red and blue dashed lines, respectively, and shaded (non-shaded) bars exceed (fall beneath) these multi-model means. The gray dashed line marked at a correlation of 0.7 is a heuristic threshold (Back et al. 2024) to decide when a particular model's MJO archetype is well captured by a model. Number of events is printed at the bottom of each bar.

To assess how closely model archetypes resemble those in reanalysis, we calculate pattern correlations between ERA5 and model time-longitude tropical OLR anomaly composites for each cluster. This evaluates how well models capture observed MJO archetypes and whether representation improves under ENSO forcing. Prior multi-model studies (Back et al. 2024) suggest a pattern correlation of 0.7 as a threshold for distinguishing well-simulated OLR Hovmöllers. For the standing MJO (Fig. 5a), five of 14 models fall below this threshold and are shaded white. Although roughly a third of simulations poorly represent the standing cluster, model skill improves during La Niña, with the multi-model mean correlation exceeding the El Niño value by 0.09. For jumping MJOs (Fig. 5b), correlations fall below 0.7 in over half the models, indicating widespread difficulty in simulating this archetype. As jumping MJOs are not thought to be ENSO sensitive, they are not analyzed further. Studies suggest slowly propagating MJOs often coincide with La Niña, though the associated SST pattern is weak and statistically insignificant (Wang et al. 2019; Back et al. 2024). Similarly, model skill is slightly higher in La Niña simulations, but likely indistinguishable from El Niño (Fig. 5c). In contrast, fast MJOs are better represented in every El Niño simulation, with the multi-model mean correlation exceeding the La Niña mean by 0.11 (Fig. 5d). In summary, model skill in representing fast and standing MJOs tends to be higher during El Niño and La Niña simulations, respectively, and models simulate a modestly higher number of fast events in their El Niño simulation.

The vertical structure of the MJO differs between slow and fast propagating events (Wang et al. 2019). To consider this further, we regress the latitudinally averaged 10°S-10°N zonal wind and temperature from ERA5 and the models onto their phase 3/4 RMM indices as in Hendon and Abhik (2018) and form pressure-longitude cross-sections (Figure 6). Phases 3/4, when the

Commented [FS24]: this figure should be updated?

Commented [de25R24]: Yes and it has been updated

Deleted: used here and elsewhere

Deleted: gauge... assess how similar the... loosely model archetypes are to... resemble those in reanalysis, we calculate pattern correlations are calculated... between the... ERA5 and model time-longitude tropical OLR convective... anomaly composites corresponding to a given... or each cluster. This measures... evaluates how well the... models represent the various... capture observed MJO archetypes and helps to assess... whether or not the... representation of a given archetype... improves in the presence of either... under ENSO forcing. Offline... prior multi-model assessments of MJO diversity... studies (Back et al. 2024) have revealed that... suggest a pattern correlation of 0.7 is... a reasonable threshold to distinguish between good and poorly... or distinguishing well-simulated OLR Hovmöllers. For the standing MJO (Fig. 5a), five of the... 4 models have correlations... all below 0.7, hence we shade their bar... his threshold and are shaded white. Although the representation of the standing cluster is poor in... oughly a third of the simulations, the representation of... poorly represent the standing MJO is notably better... luster, model skill improves during La Niña, with the multi-model pattern... can correlation exceeding its... he El Niño equivalent... alue by 0.09. The pattern correlation between the observed and simulated... or jumping MJOs falls beneath... Fig. 5b), correlations fall below 0.7 for... n over half of... he simulations... odel, indicating that the models really struggle to represent... idespread difficulty in simulating this (Fig. 5b). However,... As jumping MJOs are not currently thought to be influenced by... NSO and so... sensitive, they are not considered... analyzed further. Observations indicate that... studies suggest slowly propagating MJOs are typically concurrent... ften coincide with La Niña, however... hough associated SST pattern is weak and not... tistically significant... nsignificant (Wang et al. 2019; Back et al. 2024). Similarly, we find the representation of slowly propagating MJOs to be... odel skill is slightly better amongst the... igher in La Niña simulations, but likely statistically... ndistinguishable from the... l Niña correlations... iño (Fig. 5c). In stark... ontrast, for... ast events,... JOs are better represented in every model's... l Niño simulation represents this archetype better than the La Niña equivalent, culminating in the El Niño... with the model mean correlation exceeding the La Niña mean by 0.11 (Fig. 5d). In summary, the diversity analysis affirms that the... odel skill in representing fast and standing MJO archetypes are closely associated with... JOs tends to be higher during El Niño and La Niña simulations, respec... [51]

|

1139 MJO convection is over the western Maritime Continent, are of interest because ENSO modulates the low-frequency
1140 circulation here through its effect on the Walker Circulation, giving it a pathway to influence MJO propagation (Sun et al.
1141 2019; Suematsu and Miura 2022). Irrespective of the ENSO phase, the MJO in ERA5 exhibits a quadrupole structure in zonal
1142 wind, all of which is centered around a tropospheric warming at 140°E that peaks in amplitude near 300 hPa (cf. Jiang et al.
1143 2015).
1144

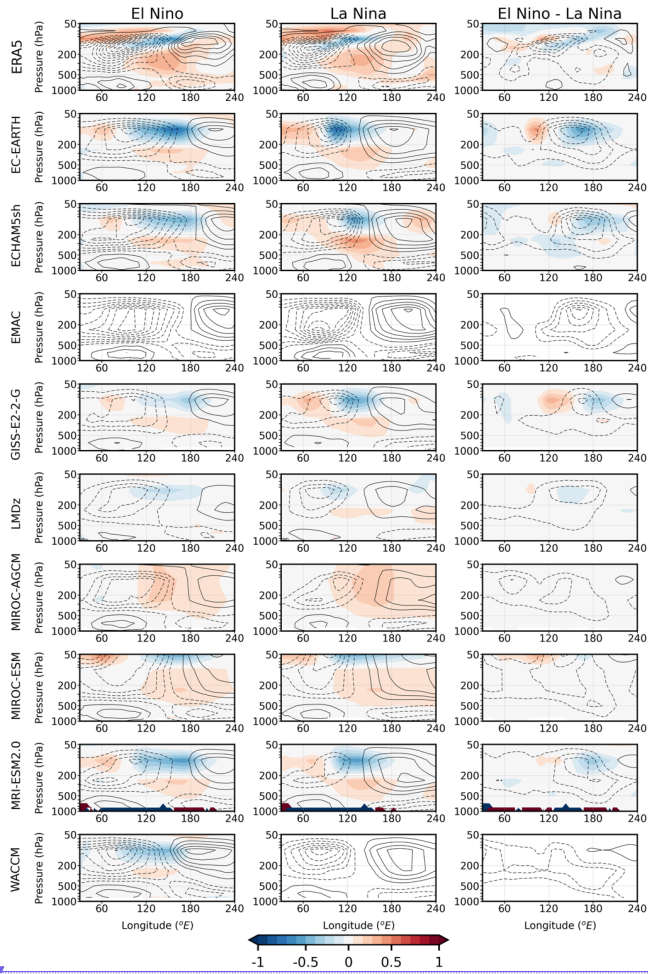
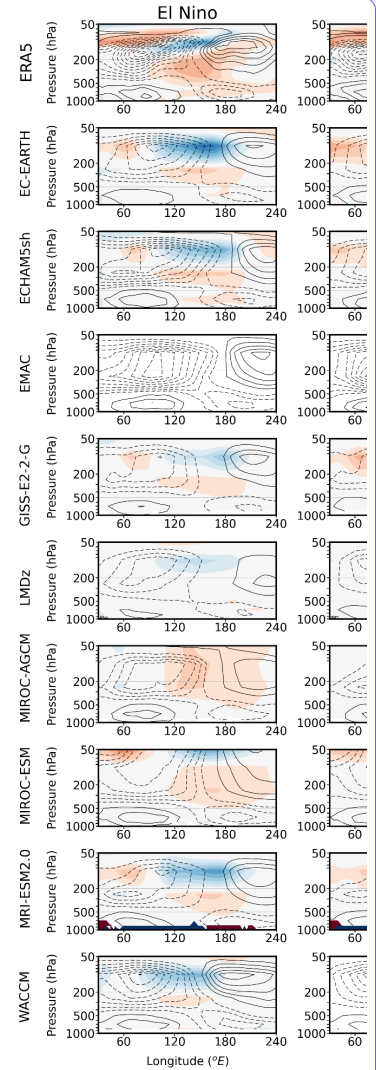


Figure 6: Pressure-longitude cross-sections of the 10°S-10°N zonal wind and temperature regressed onto the Phase 3/4 RMMs as in Hendon and Abhik (2018). Black contours show zonal wind (intervals of +/- 0.5, 1.5, 2.5 m/s...) and temperature is shaded between -1 and 1 °C. EMAC is missing temperature and we omit WACCM's La Niña temperature due to a conspicuous artifact.

Although the ERA5 El Niño and La Niña composites are similar overall, subtracting the two reveals that they differ due to the El Niño composite including a stronger Kelvin wave, evidenced by the stronger tropospheric easterlies to the east of MJO

Formatted: Header



Deleted:

Deleted: includes...ue to a conspicuous artifact that we are still looking into

[52]

1158 convection (cf. Fig. 2). In addition, the composites reveals a dry Kelvin wave signature, its characteristic features being a cold
1159 cap temperature anomaly in the UTLS, which is slightly out of phase with easterly zonal wind anomalies, all of which tilt
1160 eastward with increasing height above ~200 hPa and westward with increasing height below (Straub and Kiladis 2002; Kim
1161 et al. 2013; Yuni et al. 2019; Nakamura and Takayabu 2022). Judging by the longitude of the ERA5 100 hPa cold cap maximas,
1162 the dry Kelvin wave embedded in the composite El Niño MJO is shifted further east compared to its La Niña equivalent.

1163
1164 Consistent with recent studies, the surface easterlies positioned east of the MJO convection are indeed stronger during El Niño
1165 in reanalysis (Wang et al. 2019; Wei and Ren 2019). We attribute the amplification of these easterlies to the Kelvin wave's
1166 signature in wind, which better bridges the MJO lower tropospheric easterlies over the Pacific with the upper tropospheric
1167 easterly outflow over the Indian Ocean; compare the 500 hPa zonal winds at 150°E between El Niño and La Niña. This
1168 enhanced continuity of the MJO easterlies during El Niño is a robust feature amongst the models and is particularly clear in
1169 the El Niño minus La Niña composites of EC-EARTH3.3, ECHAM5sh, MIROC-AGCM-LL, MIROC-ESM and MRI-
1170 ESM2.0.

1171
1172 The vertical structure of the MJO zonal wind anomalies is more baroclinic during La Niña. This may be attributed to a weaker
1173 and slower propagating Kelvin wave during La Niña. However, it is also possible that the amplification of the equatorial
1174 Rossby wave during La Niña (cf. Figure 2) projects onto the MJO's vertical structure. For instance, similar to the western
1175 portion of the phase 3/4 MJO winds, these waves (when located in the eastern hemisphere) have a first baroclinic structure in
1176 zonal wind that consists of low-level westerlies and upper-level easterlies (Kiladis et al. 2009; Yuni et al. 2019; Nakamura and
1177 Takayabu 2022). Following from the robust amplification of the equatorial Rossby wave across the models during La Niña, it
1178 was hypothesized that the low-level westerlies west of the MJO convection would be stronger during La Niña than El Niño
1179 like in Wei and Ren (2019). This does not appear to be the case though and no first baroclinic zonal wind structure stands out
1180 in the El Niño minus La Niña composites. The signal of the equatorial Rossby wave does, however, appear to be visible in the
1181 temperature field. These waves are associated with a mid to upper tropospheric warming that is centered around 300 hPa
1182 (Kiladis et al. 2009, Fig. 18c). This region of the upper troposphere is warmer in all of the La Niña simulations, with the
1183 exception of MIROC-ESM in which the warming is marginally stronger in the El Niño composite.

1184 3.2 The lack of QBO-MJO interaction

1185 The results in the previous section indicate that ENSO modulates the MJO's propagation, promoting faster MJOs during El
1186 Niño and the opposite during La Niña. However, it is possible that aliased signals from the spontaneously generated QBOs are
1187 embedded in the aforementioned results. Therefore, in this section we look for evidence of QBO-MJO interaction. As a first
1188 step, the representation of the QBO is documented using previously defined metrics, with a specific interest in quantifying the
1189 "lowest level" that the QBO descends to in the lower stratosphere. Insufficient descent is a known bias, which may hinder the
1190 QBO from modulating other potentially important variables near the tropopause such as temperature (Richter et al. 2020; Kim

Formatted: Header

Deleted: The

Deleted: of the wave include its

Deleted: is in quadrature

Deleted: , evidence that it is propagating faster. This corresponds to the alignment of ERA5 Kelvin wave spectral power along the deepest equivalent depth dispersion curves during El Niño in Fig. 2.

Deleted: planetary scale

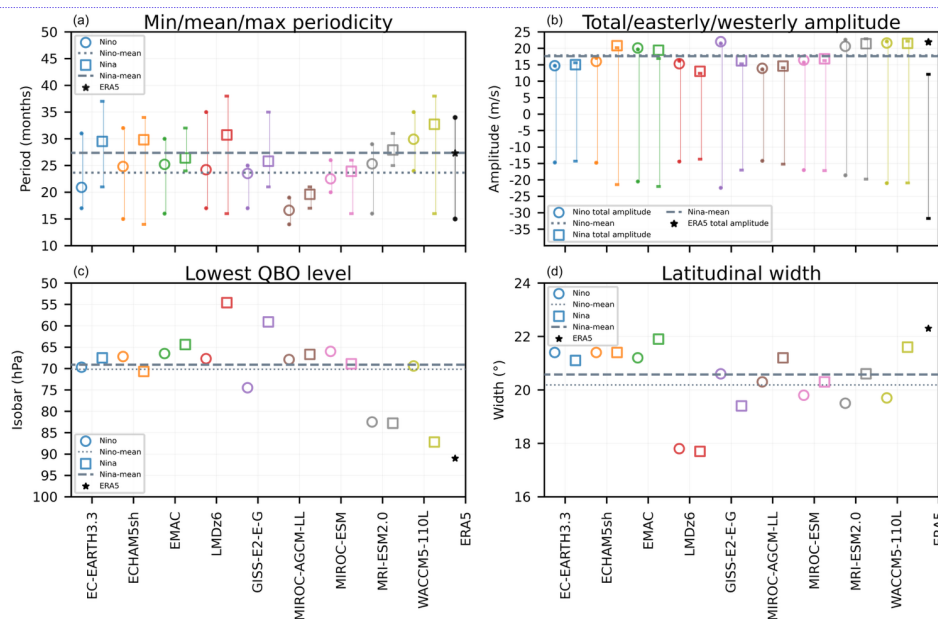
Deleted: The models, however, struggle to represent the detailed temperature structure of the Kelvin wave and they exhibit MJO temperature anomalies that can differ significantly from ERA5 (e.g., MIROC family).

Deleted: coupling

Deleted: coupling

et al. 2020). Similar to Schenzinger et al. (2017), the lowest level that QBO reaches is found by averaging the QBO Fourier amplitude (see Methods) over 5°S-5°N, identifying the maximum amplitude (fixed at 20 hPa here), and then finding the isobar in the lower stratosphere where the amplitude equals 10% of the maximum.

Formatted: Header



Deleted: Table 3: From left to right, QBO easterly, westerly, and total amplitude, the lowest level that the QBO descends to, its vertical extent, and its latitudinal extent. These statistics are computed using the same "QBO cycles" (see Methods) and QBO periodicity statistics that are reported in Kawatani et al. (2024, in preparation). Vertical extents listed as "N/A" were missing data at middle stratospheric isobars, which prevents the calculation. ECHAM5sh's El Niño simulation QBO Fourier amplitude is split into two parts above and below ~10 hPa (not shown), which is why its vertical extent is only 10.4 km.

... 531

Figure 7: Periodicity, amplitude, lowest level of descent, and latitudinal width of the QBO in El Niño (circles) and La Niña (squares) simulations. (a) mean periodicity, where whiskers extend to the minimum and maximum period. El Niño mean is dotted, La Niña mean is dashed, and ERA5 is shown in black. (b) circles and squares show total amplitudes ("TT amplitude" from Richter et al. 2020), tops of whiskers show westerly amplitudes, and bottoms of whiskers show easterly amplitudes. (c) lowest isobar the QBO descends to, the level at which the QBO Fourier amplitude falls to 10% of its maximum. (d) latitudinal width of QBO, full width at half amplitude maximum of a Gaussian fit to the QBO Fourier amplitude

Commented [FS26]: substituted by Fig 7?

Commented [de27R26]: Yes

The QBO descends to 92.2 hPa in ERA5 (Fig. 7c). Of the simulated QBOs, the majority do not reach beneath 70 hPa, indicating that they are likely too high in altitude to influence the tropical atmosphere beneath 100 hPa as observed (Tegtmeier et al. 2020). One outlier is the WACCM5-110L's La Niña simulation whose lowest isobar of 87 hPa is fairly similar to the ERA5 benchmark. Nonetheless, sensitivity tests with this simulation in which MJO amplitude is computed as a function of lower

Deleted: Table 3

1235 stratospheric QBO phase reveals its MJO to be insensitive to the QBO in the observed way (not shown), which may also be
1236 attributable to the weak MJO signal in the model. ENSO phase does not have consistent effects on what lowest isobar a given
1237 model's QBO reaches. For example, GISS-E2-2-G and LMDz6 favor much stronger descent of the QBO into the lower
1238 stratosphere during El Niño whereas WACCM5-110L's ENSO simulations reflect a strong opposite signed response.

1240 QBO periodicity varies systematically with ENSO phase in these simulations, being shorter during La Niña and longer during
1241 El Niño (Fig. 7a); see Kawatani et al. (2025) for a detailed analysis of this result. However, none of the QBO spatial metrics
1242 exhibit consistent ENSO-phase dependence across models. For example, total QBO amplitude is marginally stronger during
1243 La Niña in five of the nine models (Fig. 7b). El Niño and La Niña total QBO amplitudes differ by less than 1 m/s for all models
1244 except ECHAM5sh, GISS-E2-2-G, and LMDz6. ECHAM5sh favors a stronger QBO amplitude during La Niña, owing to
1245 intensified QBO easterlies and westerlies during this ENSO phase. Conversely, GISS-E2-2-G, and LMDz6 favor stronger
1246 easterly, westerly, and total QBO amplitudes during El Niño. Of the 12 simulations corresponding to the six other models, EC-
1247 EARTH3.3, EMAC, MIROC-AGCM-LL, MIROC-ESM, MRI-ESM2.0, and WACCM5-110L, the magnitude of their easterly
1248 and westerly QBO amplitudes is stronger during La Niña in eight of the 12 simulations. Although the models ubiquitously
1249 underestimate the latitudinal extent of the QBOs relative to ERA5, six of nine models have wider QBO latitudinal extents
1250 during La Niña (Fig. 7d). This may be noteworthy because the boreal winter polar stratospheric wind response to the QBO is
1251 stronger when the QBO is wider (Hansen et al. 2013) and there is a preference for this teleconnection to happen during La
1252 Niña over the observed record (Kumar et al. 2022).

1253
1254

Formatted: Header

Deleted: .

Deleted: E

Deleted: In general, the metrics do not change

Deleted: by

Deleted: .

Deleted: .

Deleted: EG

Deleted: EG

Deleted: The effect of ENSO phase on vertical extent is inconsistent across the models and difficult to evaluate entirely because of missing data in two models and an unrealistic QBO Fourier amplitude structure in ECHAM5sh's El Niño simulation.

Deleted: it may be noteworthy that

Deleted: . The

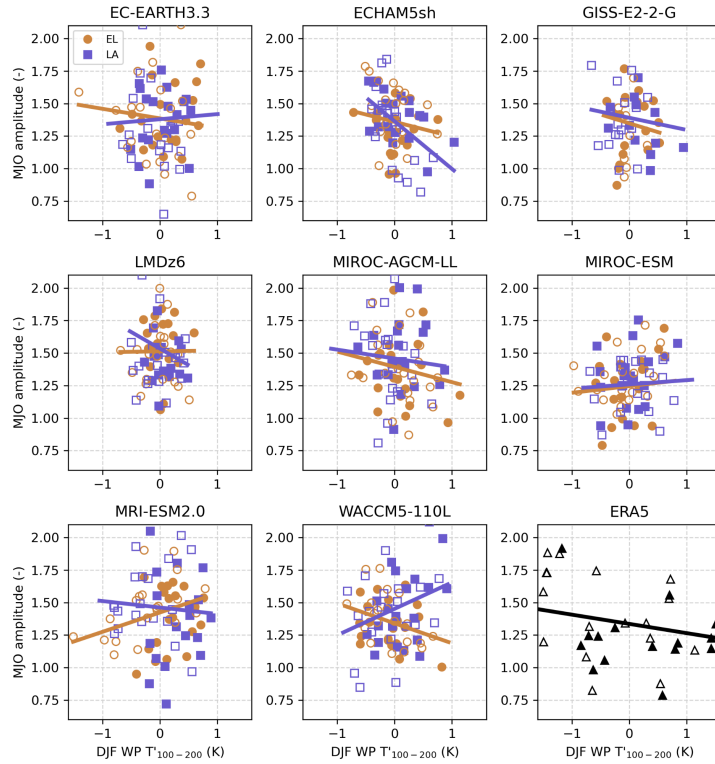


Figure 8: Scatter plot of warm-pool averaged (10°S - 10°N , 45°E - 180°E) tropopause stability anomalies (100 hPa minus 200 hPa temperature) versus December-February MJO amplitude. Lines represent the slope of the regression line during El Niño (orange) or La Niña (purple). Easterly and westerly QBO phases, which are delineated by the sign of the December-February 5°S - 5°N 50 hPa zonal mean zonal-wind, are denoted by open and filled markers, respectively.

While the aforementioned QBO metrics help to broadly characterize the form of each model's QBO, they are non-time-varying quantities and have less value for better understanding seasonal phenomena such as the predominantly boreal winter QBO-MJO interaction. To incorporate the effects of seasonality, scatterplots of December-February warm-pool averaged tropopause stability versus December-February MJO amplitude are made as a function of QBO phase for each of the simulations (Klotzbach et al. 2019). MJO amplitude is expected to increase as tropopause stability decreases (Son et al. 2017; Klotzbach et al. 2019), as is apparent based on ERA5 (Fig. 8). This metric is relevant for considering QBO-MJO coupling because the QBO's effect on lower stratospheric stability (e.g., Densmore et al. 2019) is one of the suspected physical mechanisms coupling

Commented [FS28]: this would become Fig 8 if we change the previous Table to a figure

Deleted: 7

Deleted: 7

1285 the QBO and MJO. In general, the models do not reproduce the observed inverse relation between MJO amplitude and 100-
1286 200 hPa stability and stratifying the results either by ENSO phase or QBO phase does not change this. The linear response of
1287 the MJO amplitude to the tropopause stability, which is negative in observations, does not change consistently with the ENSO
1288 phase. It is worth noting that the mean DJF stability in the models is generally close to that of ERA5 (-28.7 K) except for the
1289 GISS model, which showcases a smaller gradient (-23.3 K), and all models appear to underestimate its interannual variability,
1290 as evident by the smaller range compared to ERA5, (recall however that imposed SSTs do not vary interannually). Furthermore,
1291 the stratification by QBO phase (with EQBO associated with lower stability values, and vice versa for the WQBO) is also
1292 small or absent in models, possibly due to a limited influence of the QBO at tropopause heights (Serva et al., 2022). Further
1293 sensitivity tests were done to see if the model QBOs simulate a QBO-MJO amplitude relationship when the MJO is in a
1294 particular phase (e.g., Lim and Son 2020; Lawrence et al. 2023); no systematic effect was detected (not shown).

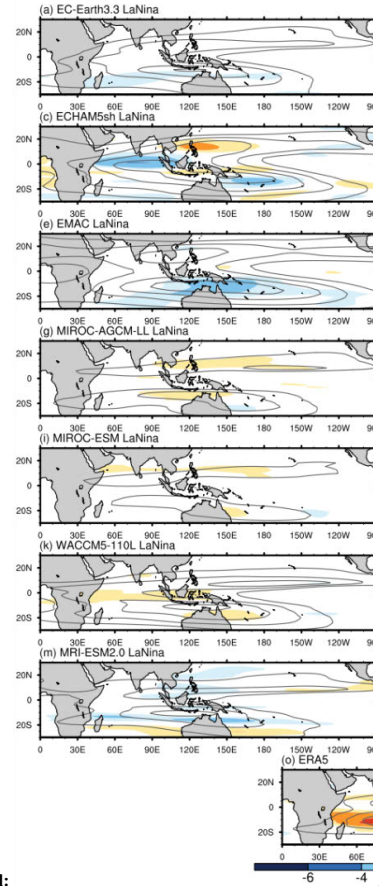
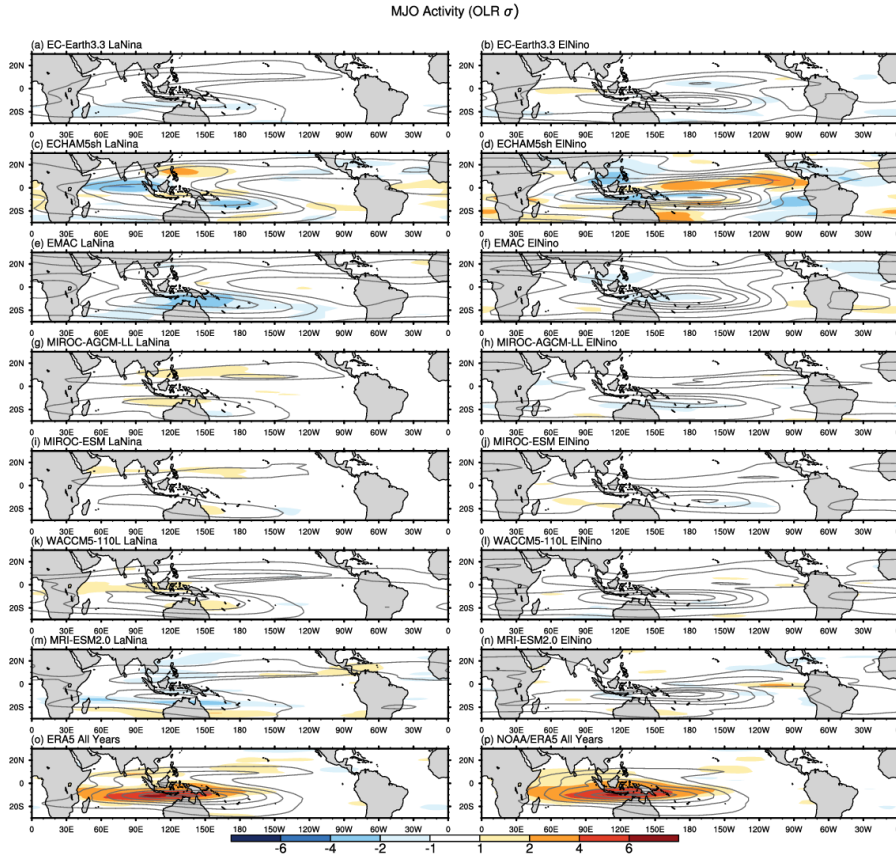
Formatted: Header

Deleted: .

Deleted: eQBO

Deleted: wQBO

Formatted: Header



Deleted:

Deleted: 8

Commented [FS29]: at which level? It is interesting to note that ECHMA5sh QBO in EL tends to stall - similar thing happening in GISS during LA. check Fig 2 <https://egusphere.copernicus.org/preprints/2024/egusphere-2024-3270/egusphere-2024-3270.pdf>

Commented [FS30R29]: but since GISS is missing (I guess because it has no OLR) I think we can't conclude much

Commented [de31R29]: added 50 hPa as level. See Methods too. We now have two mentions (L605, L647) of basic state wind biases associated with the QBO

Deleted: 8

1298
1299 **Figure 9:** Gray contours show the MJO activity defined as the standard deviation of MJO-filtered OLR for each model and ENSO
1300 phase, as well as for ERA5 (6n). The color-filled contours show the MJO-QBO relationship as the difference in MJO activity for the
1301 eastward minus westward 50 hPa QBO phases for each model and ERA5.

1302 To further evaluate the representation of QBO-MJO coupling in the models, Figure 9 presents the effect of QBO phase on
1303 MJO activity (see Methods). As shown in previous studies (e.g., Kim et al. 2020), the models do not capture the observed

QBO-MJO relationship, which has maximum signal over the maritime continent region (Fig. 9m) illustrating the enhancement of MJO activity during easterly QBO phase. With La Niña forcing, MIROC-AGCM-LL and WACCM5-110L show a weak positive signal over the Maritime Continent (Fig. 9g, k), however EC-EARTH3.3, ECHAM5sh, and EMAC exhibit rather different responses. In MIROC models, the MJO activity is further shifted off-equator, possibly hampering any QBO control on MJO convection. No change in the MJO activity by QBO phase is evident in the El Niño simulations either, except for some negative signal in the central and eastern Pacific in ECHAM5sh, which may be due to an irregular QBO in this experiment (Kawatani et al., 2025). There is, however, a clear eastward shift of the MJO activity towards the Pacific during El Niño, corroborating the observational work of Kessler (2001) and the climate model based study of Tam and Lau (2005).

4 Discussion and conclusions

The observed interannual variability of the MJO is influenced by multiple parts of the climate system. Due to their impact on the tropical troposphere and prominent fluctuations at interannual timescales, ENSO and the QBO are known drivers of the MJO's year to year variability, however it is difficult to definitively isolate their influence on the MJO because of how short and noisy the observational record is (Randall et al. 2023). Building on previous work, our aim here is to evaluate the extent to which model behavior is consistent with previously reported ENSO-MJO relationships by analyzing the representation of the MJO in nine climate models forced by prescribed perpetual El Niño and La Niña conditions, each with a spontaneously generated QBO. While the imposed SST anomalies represent an upper bound for the observed record, they are relevant given the projected intensity increase of ENSO extremes.

Although the models exhibit difficulties simulating the MJO, several previously reported effects of the ENSO phase on the MJO are corroborated by this coordinated set of experiments. These effects include faster propagation of the MJO during El Niño versus slower propagation during La Niña, manifesting as shorter and longer lifetimes, respectively, stronger amplitude of the MJO during El Niño, and east-west shifting of the MJO timescale variance towards the east Pacific during El Niño and towards the west Pacific and Indian Ocean during La Niña. It is likely that the high-amplitude SST forcings used here, particularly the amplified El Niño forcing, contribute to the magnitude of these ENSO associated MJO changes, consistent with prior work linking exceptionally warm Pacific SSTs to enhanced or farther-east MJO propagation (e.g., Marshall et al. 2016). To assess this sensitivity to ENSO amplitude, we compare a broad measure of MJO quality and propagation, the MJO E/W ratio, between the perpetual ENSO simulations and each model's 1979–2009 AMIP simulations, which are more representative of typical ENSO amplitudes. Across models, El Niño forcing increases the E/W ratio, often pushing it toward the upper tail of the AMIP-based internal variability distribution, indicating more robust eastward MJO propagation, whereas many La Niña simulations produce ratios near unity. Notably, all perpetual ENSO E/W ratios remain within the spectrum of their AMIP-based values, underscoring that the modeled responses, while produced by extreme forcings, do not exceed the range of variability seen under more normal SSTs. We note that, besides SSTs, the representation of MJOs in models appears

Formatted: Header

Deleted: 8m

Deleted: 8g

Deleted: .

Deleted: we have analyzed

Deleted: that are

Deleted:

Deleted:

Deleted: and which include

Deleted: QBOs.

1349 to be particularly sensitive to convective schemes, as discussed by Rind et al. (2020) for GISS, by Park et al. (2019) for
1350 WACCM, by Miura et al. (2012) for MIROC and Holt et al. (2020) for other Phase 1 QBOi models. The impact of the
1351 convective scheme, for example, appears oversized compared to horizontal resolution, which is finely resolved in EC-
1352 EARTH3.3, MIROC-AGCM-LL, MRI-ESM2.0, and WACCM, none of which are exceptional at reproducing the MJO's
1353 wavenumber frequency spectra or E/W ratios. Moreover, models within the same family (MIROC-based, ECHAM-based)
1354 exhibit similar MJO spectra (Fig. 2, Fig. 4), despite having intra-family differences in horizontal and vertical resolution (Table
1355 2; Holt et al. 2020, Fig. 18). As shown by Orbe et al. (2020) for the WACCM and GISS models, refinement of key
1356 parameterization has potential to improve simulated MJOs.

1358 As in the observational record, it is possible that aliasing from the QBO is superimposed on what are thought to be MJO
1359 changes due to ENSO. However, we find that the climate models considered here show little evidence of QBO-MJO coupling.
1360 This may be due to various factors, such as biases in the descent of the QBO, and the location and characteristics of tropical
1361 convection, which appears to be less organized in some of the models compared to GPCP. While this limits our ability to
1362 diagnose the mechanisms linking the QBO and MJO, it suggests that, in these experiments, the MJO changes we detect are
1363 primarily driven by the ENSO forcings. Experiments with specified rather than internally generated QBO aspects can help
1364 understanding the processes at play, which remain elusive (Martin et al., 2023; Huang et al. 2023). One speculative reason for
1365 the missing QBO-MJO signal is the representation of Kelvin waves. Observations show that during EQBO, the Kelvin wave
1366 associated with MJO penetrates higher into the lower stratosphere, coinciding with an eastward-tilting cold anomaly in the
1367 UTLS (Hendon and Abhik 2018). We find a similar dry Kelvin wave signature in our ERA5 El Niño minus La Niña MJO
1368 vertical structure composite, but in models, the UTLS wave structure is much more coarsely resolved (Fig. 6). Such
1369 deficiencies, perhaps linked to vertical resolution (Holt et al. 2020, Fig. 18a), lower-stratospheric wind biases that develop in
1370 the absence of sufficient QBO descent (Fig. 7c), or perhaps just weak MJOs, may weaken this dry Kelvin wave component
1371 and, in turn, suppress QBO-MJO interaction.

1373 These results highlight that the interannual variability of the MJO is sensitive to ENSO in several regards, in contrast with
1374 Slingo et al. (1999) and Hendon et al. (1999). These studies reported a weak simultaneous relationship between ENSO and
1375 MJO activity. Hendon et al. (1999) found that increased MJO activity coincides with an increased number of MJO events and
1376 enhanced intraseasonal convective activity around the Maritime Continent. While these attributes of the MJO were largely
1377 insensitive to SSTs in their study, the models here unambiguously simulate more events in their perpetual El Niño simulation
1378 (Table 2), which are of stronger MJO activity than their La Niña equivalents (Figure 8). We suspect that the distinction between
1379 our results and the previous research is related to the timescale over which the oceanic component of ENSO modulates the
1380 atmosphere. Recent studies show that while the likelihood of MJO occurrence and its propagation speed are only weakly
1381 correlated with tropical intraseasonally filtered SSTs, they are strongly correlated with low-frequency (e.g., > 90 days) SSTs
1382 (Suematsu and Miura 2018; 2022). Along the same lines, Newman et al. (2009) found air-sea coupling to have weak effects

Formatted: Header

Commented [FS32]: do we add this?
<https://journals.ametsoc.org/view/journals/clim/33/17/jcliD190956.pdf>

Commented [de33R32]: Yes - nice addition!

Deleted: include nearly no

Commented [FS34]: related to spectrum shifts in wavenumber

Commented [de35R34]: Yeah, I think is valid based on Fig 2/4

Deleted: hampers further understanding of

Deleted: responsible for coupling

Deleted: in all likelihood this eliminates the QBO as a driver of the MJO in this set of

Deleted: which increases our confidence that the aforementioned ...

Deleted: in the MJO

Deleted: arising due to

Deleted: QBOs

Deleted: .)

Commented [FS36]: I guess we can be more explicit and stress how the realism of MJO (perhaps through convective organization or vertical depth of convection) determine the realism of the response. It is perhaps trivial but examples of LMDz6 and GISS could be repeated. Need to find suitable references!

Commented [FS37R36]: As a perspective, I guess we could add that improving the MJO representation seems to be important

Commented [de38R36]: I alluded to the importance of improving the MJOs in P1 and P2 of the conclusions rather than here in paragraph three (P3)

Deleted: clarified

Deleted: during

Deleted: aforementioned studies

Deleted: (agreeing with the aforementioned studies),

1398 on subseasonal atmospheric variability, but strong influence on the long-term atmospheric circulation. In light of this and our
1399 use of a simplified climate system in which smoothed monthly SSTs are prescribed, intraseasonal and interannual SST
1400 fluctuations are explicitly ignored, and the downward impact of the MJO on intraseasonal SSTs (Zhang and Gottschalk 2002;
1401 Hendon et al. 2007; Newman et al. 2009) is not simulated, we deduce that the different basic state circulations set up by the
1402 indefinite ENSO forcings enables distinct MJOs. This interpretation of the low-frequency SSTs as an important modulator of
1403 the MJO aligns with studies which have attributed variability in the MJO's propagation to ENSO (Wei and Ren 2019; Wang
1404 et al. 2019; Dasgupta et al. 2021; Back et al. 2024) as well as studies employing climate models in which MJO propagation
1405 can be modulated by changing the horizontal gradients of the background SST field (Kang et al. 2013; Jiang et al. 2020).

1406
1407 Compared with the La Niña simulations, all El Niño simulations include amplified Kelvin waves whereas equatorial Rossby
1408 waves intensify in the presence of perpetual La Niña conditions. Consistent with the reported relationship between the these
1409 wave and the MJO (Wei and Ren 2019), all models simulate faster MJO propagation in their El Niño simulation. This is further
1410 supported by the MJO diversity analysis, which reveals that models reproduce the observed fast and standing MJO archetype
1411 OLR Hovmöllers well in the presence of perpetual El Niño and La Niña conditions, respectively. In addition, the MJO's phase
1412 3/4 vertical structures highlight that lower tropospheric easterlies do intensify to the east of the MJO's major convection during
1413 El Niño across most models, which we interpret to result from the intensification of the Kelvin wave.

1414
1415 While the relationship between Kelvin waves, equatorial Rossby waves, and ENSO is well established by previous studies
1416 employing empirical data and reanalysis, this is the first time, to the best of our knowledge, that this relationship has been
1417 ubiquitously affirmed by a coordinated set of climate model experiments with prescribed strong ENSO forcings. The
1418 robustness of this result across models suggests that it is worthwhile considering how these wave responses to ENSO influence
1419 other parts of the climate system. For instance, Kelvin waves are a source of resolved wave forcing for the QBO (Baldwin et
1420 al. 2001; Taguchi 2010; Pahlavan et al. 2021) and more rapid descent of the QBO's westerly shear zones during El Niño in
1421 observations has been attributed to their intensification (Das and Pan 2016). The periodicity of the QBO in the El Niño
1422 simulations is in fact shorter than in the La Niña simulations across all models considered here (Kawatani et al., 2025),
1423 however, the extent to which Kelvin waves are responsible for this as opposed to other waves (e.g., Kawatani et al. 2019), is
1424 yet to be quantified across all of the models. The convectively coupled wave responses presented here may also be relevant
1425 for better understanding ENSO diversity. El Niño events vary in type and intensity due to the influence of westerly wind bursts,
1426 which introduce asymmetry and irregularity into ENSO's phase changes (Chen et al. 2015). Westerly wind bursts are more
1427 frequent during the convective phases of equatorial Rossby waves and the MJO, especially strong MJOs (Puy et al. 2016).
1428 Hence, the atmospheric responses to ENSO, such as the amplifications of the MJO during El Niño (Figs. 2-4) and of the
1429 convectively coupled Rossby wave during La Niña, have a pathway to influence ENSO's oceanic component.

1430
1431 **Code availability**

Formatted: Header

Commented [FS39]: there were comment on dry waves etc....to be implemented better

Commented [de40R39]: I simply mentioned "dry kelvin wave signature" above where relevant, but don't want to dive too much into this

Commented [de41R39]: I did revise the text beneath Figure 6, where the reviewer made their comment, to contrast the dry vs. convectively coupled kelvin wave

Commented [FS42]: I think we should add a sentence or two on why these are better than MJOs

Commented [FS43R42]: based on Holt 2020, I guess the motivation is that these are larger and somewhat less sensitive to physical schemes, but mostly depend on model resolution and systematic dynamical biases

Commented [de44R42]: I omitted this because it's complicated. The sensitivity of MJO E/W ratios to the El Niño v La Niña forcing is actually stronger than the sensitivity of the Kelvin or Eq Rossby waves to the El Niño v La Niña forcings. E.g., ECHAM5sh's ratio of El Niño to La Niña E/W ratio (yes, its the ratio of a ratio) is ~ 1.8, whereas its El Niño to La Niña Kelvin and ER spectral power ratios are 1.15 and 0.85. This is true for most models and suggests that MJO propagation is more impacted by the forcing that either of the convectively coupled waves

Deleted: waves

Deleted: ,

Deleted: simulate

Deleted: archetypes

Commented [FS45]: indeed following the reviewers I'd add here a paragraph on the (lack of) QBO MJO connection

Commented [FS46R45]: The fact that Huang stresses temperature makes me wonder if convection characteristics also matters

Commented [de47R45]: I added the Huang reference with the Martin et al. 2023 reference in Conclusions section paragraph 2. I also added speculations on the lack of QBO-MJO coupling there

Deleted: in preparation

Commented [FS48]: update if needed

Formatted: Header

1437

1438 The code used for the wavenumber-frequency analysis is publicly available through the National Center for Atmospheric
1439 Research (NCAR) Command Language (NCL): <https://www.ncl.ucar.edu/Applications/mjoelivar.shtml>. A reproduction of
1440 NCL's Wheeler-Kiladis (1999) routine in Python is available here: https://github.com/brianpm/wavenumber_frequency.
1441 Python code, which assesses QBO morphology is available here: [https://github.com/NOAA-GFDL/MDTF-](https://github.com/NOAA-GFDL/MDTF-diagnostics/blob/main/diagnostics/stc_qbo_ens0/stc_qbo_ens0.py)
1442 [diagnostics/blob/main/diagnostics/stc_qbo_ens0/stc_qbo_ens0.py](https://github.com/NOAA-GFDL/MDTF-diagnostics/blob/main/diagnostics/stc_qbo_ens0/stc_qbo_ens0.py).

1443

1444 **Data availability**

1445 Storage for the QBOi multi-model data set is provided by the Centre for Environmental Data Analysis (CEDA) whose data
1446 and processing service is called JASMIN. Interested users must obtain a JASMIN login account and take the necessary steps
1447 to access the QBOi group workspace within JASMIN, which contains the perpetual ENSO simulations. Certain derived model
1448 products (e.g., the MJO RMMs) may be made available upon request.

1449

1450 **Author contributions**

1451 DE, FS, JC, SYB, CO, and JR contributed to the conceptualization of this study. DE, FS, JC, and SYB performed the data
1452 analyses and produced the figures and tables. All authors contributed to the review and editing of this manuscript.

1453

1454 **Competing interests**

1455 The authors declare that they have no conflict of interest.

1456

1457 **Acknowledgements**

1458 DE was supported in part by NOAA Cooperative Agreement NA22OAR4320151 and appreciates helpful discussions with
1459 John Albers, Juliana Dias, George Kiladis, Matthew Newman, Brandon Wolding, and Amy Butler. The ECHAM5sh
1460 simulations were performed thanks to an ECMWF Special Project awarded to FS. YK[KY1] was supported by JSPS
1461 KAKENHI (JP22K18743) and the Environment Research and Technology Development Fund (JPMEERF20242001) of the
1462 Environmental Restoration and Conservation Agency provided by Ministry of the Environment of Japan. YK and SW were
1463 supported by JSPS KAKENHI (JP22H01303 and JP23K22574). SW was supported by MEXT-Program for the advanced
1464 studies of climate change projection (SENTAN) Grant Number JPMXD0722681344. [S.-W. Son was supported by a grant](#)
1465 [from the National Research Foundation of Korea \(NRF\), funded by the Korean government \(MSIT\) \(2023R1A2C3005607\).](#)
1466 [NB was funded by the Met Office Climate Science for Service Partnership \(CSSP\) China project under the International](#)
1467 [Science Partnerships Fund \(ISPF\).](#) The numerical simulations of MIROC models were performed using the Earth Simulator.
1468 The GFD-DENNOU Library and GrADS were used to draw the figures. TK and SV acknowledge support by the state of
1469 Baden-Württemberg through bwHPC. Portions of this work were supported by the National Center for Atmospheric Research
1470 (NCAR), which is a major facility sponsored by the National Science Foundation (NSF) under Cooperative Agreement

Commented [FS49]: also Amy?

Commented [de50R49]: added amy

Deleted: and

1472 1852977. Portions of this study were supported by the Regional and Global Model Analysis (RGMA) component of the Earth
1473 and Environmental System Modeling Program of the U.S. Department of Energy's Office of Biological and Environmental
1474 Research (BER) via NSF Interagency Agreement 1844590. The authors gratefully acknowledge the UK Centre for
1475 Environmental Data Analysis for providing [archival and analysis resources](#) for the QBOi multimodel dataset.

1477 **References**

1479 [Adler, Robert; Wang, Jian-Jian; Sapiano, Mathew; Huffman, George; Bolvin, David; Nelkin, Eric; and NOAA CDR Program
1480 \(2017\). Global Precipitation Climatology Project \(GPCP\) Climate Data Record \(CDR\), Version 1.3 \(Daily\) \[1996-2022\].
1481 NOAA National Centers for Environmental Information. doi:10.7289/V5RX998Z \[July 2025\]](#)

1482 [Ahn, M.-S., Kim, D., Sperber, K. R., Kang, I.-S., Maloney, E., Waliser, D., and Hendon, H.: MJO simulation in CMIP5 climate
1483 models: MJO skill metrics and process-oriented diagnosis, Clim Dyn, 49, 4023–4045, \[https://doi.org/10.1007/s00382-017-
1485 3558-4\]\(https://doi.org/10.1007/s00382-017-
1484 3558-4\), 2017.](#)

1486 [Ahn, M., Kim, D., Kang, D., Lee, J., Sperber, K. R., Gleckler, P. J., Jiang, X., Ham, Y., and Kim, H.: MJO Propagation Across
1487 the Maritime Continent: Are CMIP6 Models Better Than CMIP5 Models?, Geophysical Research Letters, 47,
1488 e2020GL087250, <https://doi.org/10.1029/2020GL087250>, 2020.](#)

1489 [Back, S.-Y., Kim, D., and Son, S.-W.: MJO Diversity in CMIP6 Models, Journal of Climate, 37, 4835–4850,
1490 <https://doi.org/10.1175/JCLI-D-23-0656.1>, 2024.](#)

1491 [Baldwin, M. P., Gray, L. J., Dunkerton, T. J., Hamilton, K., Haynes, P. H., Randel, W. J., Holton, J. R., Alexander, M. J.,
1492 Hirota, I., Horinouchi, T., Jones, D. B. A., Kinnersley, J. S., Marquardt, C., Sato, K., and Takahashi, M.: The quasi-biennial
1493 oscillation, Reviews of Geophysics, 39, 179–229, <https://doi.org/10.1029/1999RG000073>, 2001.](#)

1494 [Bechtold, P., Semane, N., Lopez, P., Chaboureaud, J.-P., Beljaars, A., and Bormann, N.: Representing Equilibrium and
1495 Nonequilibrium Convection in Large-Scale Models, Journal of the Atmospheric Sciences, 71, 734–753,
1496 <https://doi.org/10.1175/JAS-D-13-0163.1>, 2014.](#)

1497 [Berrington, A. H., Sakaeda, N., Dias, J., and Kiladis, G. N.: Relationships Between the Eastward Propagation of the Madden-
1498 Julian Oscillation and Its Circulation Structure, JGR Atmospheres, 127, e2021JD035806,
1499 <https://doi.org/10.1029/2021JD035806>, 2022.](#)

1500 [Bushell, A. C., Anstey, J. A., Butchart, N., Kawatani, Y., Osprey, S. M., Richter, J. H., Serva, F., Braesicke, P., Cagnazzo, C.,
1501 Chen, C.-C., Chun, H.-Y., Garcia, R. R., Gray, L. J., Hamilton, K., Kerzenmacher, T., Kim, Y.-H., Lott, F., McLandress, C.,
1502 Naoe, H., Scinocca, J., Smith, A. K., Stockdale, T. N., Versick, S., Watanabe, S., Yoshida, K., and Yukimoto, S.: Evaluation
1503 of the Quasi-Biennial Oscillation in global climate models for the SPARC QBO-initiative, Quart J Royal Meteor Soc, 148,
1504 1459–1489, <https://doi.org/10.1002/qj.3765>, 2022.](#)

1505 [Butchart, N., Anstey, J. A., Hamilton, K., Osprey, S., McLandress, C., Bushell, A. C., Kawatani, Y., Kim, Y.-H., Lott, F.,
1506 Scinocca, J., Stockdale, T. N., Andrews, M., Bellprat, O., Braesicke, P., Cagnazzo, C., Chen, C.-C., Chun, H.-Y., Dobrynin,
1507 M., Garcia, R. R., Garcia-Serrano, J., Gray, L. J., Holt, L., Kerzenmacher, T., Naoe, H., Pohlmann, H., Richter, J. H., Scaife,
1508 A. A., Schenzinger, V., Serva, F., Versick, S., Watanabe, S., Yoshida, K., and Yukimoto, S.: Overview of experiment design
1509 and comparison of models participating in phase 1 of the SPARC Quasi-Biennial Oscillation initiative \(QBOi\), Geosci. Model
1510 Dev., 11, 1009–1032, <https://doi.org/10.5194/gmd-11-1009-2018>, 2018.](#)

1518

Formatted: Header

Deleted: resourcing

Commented [FS51]: to do: cross-check all refs with the text before submission

Formatted: Font: Bold

Formatted: Line spacing: single

Commented [FS52]: first one should be Adler of any GPCP ref

Commented [FS53R52]: please Dillon confirm the version

Commented [de54R52]: V1.3 - see thread above

- 1520 Chen, D., Lian, T., Fu, C., Cane, M. A., Tang, Y., Murtugudde, R., Song, X., Wu, Q., and Zhou, L.: Strong influence of
1521 westerly wind bursts on El Niño diversity, *Nature Geosci*, 8, 339–345, <https://doi.org/10.1038/ngeo2399>, 2015.
1522
- 1523 Chikira, M. and Sugiyama, M.: A Cumulus Parameterization with State-Dependent Entrainment Rate. Part I: Description and
1524 Sensitivity to Temperature and Humidity Profiles, *Journal of the Atmospheric Sciences*, 67, 2171–2193,
1525 <https://doi.org/10.1175/2010JAS3316.1>, 2010.
1526
- 1527 Das, U. and Pan, C. J.: Equatorial atmospheric Kelvin waves during El Niño episodes and their effect on stratospheric QBO,
1528 *Science of The Total Environment*, 544, 908–918, <https://doi.org/10.1016/j.scitotenv.2015.12.009>, 2016.
1529
- 1530 Dasgupta, P., Roxy, M. K., Chattopadhyay, R., Naidu, C. V., and Metya, A.: Interannual variability of the frequency of MJO
1531 phases and its association with two types of ENSO, *Sci Rep*, 11, 11541, <https://doi.org/10.1038/s41598-021-91060-2>, 2021.
1532
- 1533 Densmore, C. R., Sanabia, E. R., and Barrett, B. S.: QBO Influence on MJO Amplitude over the Maritime Continent: Physical
1534 Mechanisms and Seasonality, *Monthly Weather Review*, 147, 389–406, <https://doi.org/10.1175/MWR-D-18-0158.1>, 2019.
1535
- 1536 Emanuel, K. A.: A Scheme for Representing Cumulus Convection in Large-Scale Models, *J. Atmos. Sci.*, 48, 2313–2329,
1537 [https://doi.org/10.1175/1520-0469\(1991\)048<2313:ASFRCC>2.0.CO;2](https://doi.org/10.1175/1520-0469(1991)048<2313:ASFRCC>2.0.CO;2), 1991.
1538
- 1539 Emori, S., Nozawa, T., Numaguti, A., and Uno, I.: Importance of Cumulus Parameterization for Precipitation Simulation over
1540 East Asia in June., *Journal of the Meteorological Society of Japan*, 79, 939–947, <https://doi.org/10.2151/jmsj.79.939>, 2001.
1541
- 1542 Fernandes, L. G. and Grimm, A. M.: ENSO Modulation of Global MJO and Its Impacts on South America, *Journal of Climate*,
1543 36, 7715–7738, <https://doi.org/10.1175/JCLI-D-22-0781.1>, 2023.
1544
- 1545 [Gehne, M., Hamill, T. M., Kiladis, G. N., and Trenberth, K. E.: Comparison of Global Precipitation Estimates across a Range
1546 of Temporal and Spatial Scales. *Journal of Climate*, 29\(21\), 7773–7795. <https://doi.org/10.1175/JCLI-D-15-0618.1>, 2016.](https://doi.org/10.1175/JCLI-D-15-0618.1)
1547
- 1548 Hendon, H. H. and Abhik, S.: Differences in Vertical Structure of the Madden-Julian Oscillation Associated With the Quasi-
1549 Biennial Oscillation, *Geophysical Research Letters*, 45, 4419–4428, <https://doi.org/10.1029/2018GL077207>, 2018.
1550
- 1551 Ham, S. and Hong, S.-Y.: Sensitivity of simulated intraseasonal oscillation to four convective parameterization schemes in a
1552 coupled climate model, *Asia-Pacific J Atmos Sci*, 49, 483–496, <https://doi.org/10.1007/s13143-013-0043-9>, 2013.
1553
- 1554 Hansen, F., Matthes, K., and Gray, L. J.: Sensitivity of stratospheric dynamics and chemistry to QBO nudging width in the
1555 chemistry–climate model WACCM, *JGR Atmospheres*, 118, <https://doi.org/10.1002/jgrd.50812>, 2013.
1556
- 1557 Hendon, H. H. and Salby, M. L.: The Life Cycle of the Madden–Julian Oscillation, *J. Atmos. Sci.*, 51, 2225–2237,
1558 [https://doi.org/10.1175/1520-0469\(1994\)051<2225:TLCOTM>2.0.CO;2](https://doi.org/10.1175/1520-0469(1994)051<2225:TLCOTM>2.0.CO;2), 1994.
1559
- 1560 Hendon, H. H., Zhang, C., and Glick, J. D.: Interannual Variation of the Madden–Julian Oscillation during Austral Summer,
1561 *J. Climate*, 12, 2538–2550, [https://doi.org/10.1175/1520-0442\(1999\)012<2538:IVOTMJ>2.0.CO;2](https://doi.org/10.1175/1520-0442(1999)012<2538:IVOTMJ>2.0.CO;2), 1999.
1562
- 1563 Hendon, H. H., Wheeler, M. C., and Zhang, C.: Seasonal Dependence of the MJO–ENSO Relationship, *Journal of Climate*,
1564 20, 531–543, <https://doi.org/10.1175/JCLI4003.1>, 2007.
1565
- 1566 Henley, B. J., Gergis, J., Karoly, D. J., Power, S., Kennedy, J., and Folland, C. K.: A Tripole Index for the Interdecadal Pacific
1567 Oscillation, *Clim Dyn*, 45, 3077–3090, <https://doi.org/10.1007/s00382-015-2525-1>, 2015.
1568

Hourdin, F., Grandpeix, J.-Y., Rio, C., Bony, S., Jam, A., Cheruy, F., Rochetin, N., Fairhead, L., Idelkadi, A., Musat, I., Dufresne, J.-L., Lahellec, A., Lefebvre, M.-P., and Roehrig, R.: LMDZ5B: the atmospheric component of the IPSL climate model with revisited parameterizations for clouds and convection, *Clim Dyn*, 40, 2193–2222, <https://doi.org/10.1007/s00382-012-1343-y>, 2013.

Huang, K., Richter, J. H., and Pegion, K. V.: Captured QBO-MJO Connection in a Subseasonal Prediction System, *Geophysical Research Letters*, 50, e2022GL102648, <https://doi.org/10.1029/2022GL102648>, 2023.

Huffman, G.J., R.F. Adler, M. Morrissey, D.T. Bolvin, S. Curtis, R. Joyce, B McGavock, J. Susskind: *Global Precipitation at One-Degree Daily Resolution from Multi-Satellite Observations*. *J. Hydrometeor.*, 2(1), 36-50, doi.org/10.1175/1525-7541(2001)002<0036:GPAODD>2.0.CO;2, 2001

Jiang, X., Waliser, D. E., Xavier, P. K., Petch, J., Klingaman, N. P., Woolnough, S. J., Guan, B., Bellon, G., Crueger, T., DeMott, C., Hannay, C., Lin, H., Hu, W., Kim, D., Lappen, C., Lu, M., Ma, H., Miyakawa, T., Ridout, J. A., Schubert, S. D., Scinocca, J., Seo, K., Shindo, E., Song, X., Stan, C., Tseng, W., Wang, W., Wu, T., Wu, X., Wyser, K., Zhang, G. J., and Zhu, H.: Vertical structure and physical processes of the Madden-Julian oscillation: Exploring key model physics in climate simulations, *JGR Atmospheres*, 120, 4718–4748, <https://doi.org/10.1002/2014JD022375>, 2015.

Jiang, X., Maloney, E., and Su, H.: Large-scale controls of propagation of the Madden-Julian Oscillation, *npj Clim Atmos Sci*, 3, 29, <https://doi.org/10.1038/s41612-020-00134-x>, 2020.

Jin, D., D. Kim, S.-W. Son, and L. Oreopoulos, 2023: QBO deepens MJO convection, *Nature Communications*, 14, 4088, <https://doi.org/10.1038/s41467-023-39465-7>

Kang, I.-S., Liu, F., Ahn, M.-S., Yang, Y.-M., and Wang, B.: The Role of SST Structure in Convectively Coupled Kelvin–Rossby Waves and Its Implications for MJO Formation, *Journal of Climate*, 26, 5915–5930, <https://doi.org/10.1175/JCLI-D-12-00303.1>, 2013.

Kawatani, Y., Hamilton, K., Sato, K., Dunkerton, T. J., Watanabe, S., and Kikuchi, K.: ENSO Modulation of the QBO: Results from MIROC Models with and without Nonorographic Gravity Wave Parameterization, *Journal of the Atmospheric Sciences*, 76, 3893–3917, <https://doi.org/10.1175/JAS-D-19-0163.1>, 2019.

Kawatani, Y., Hamilton, K., Watanabe, S., M., Taguchi, Serva, F., Anstey, J. A., Richter, J. H., Butchart, N., Orbe, C., Osprey, S. M., Naoe, H., Elsbury, D., Chen, C.-C., Garcia-Serrano, J., Glanville, A., Kerzenmacher, T., Lott, F., Palmeiro, F. M., Park, M., Versick, S., and Yoshida, K.: QBO El Nino Southern Oscillation experiments Part I: Overview of experiment design and ENSO modulation of the QBO, *Weather and Climate Dynamics* (in press), <https://doi.org/10.5194/egusphere-2024-3270-2025>.

Kelley, M., Schmidt, G. A., Nazarenko, L. S., Bauer, S. E., Ruedy, R., Russell, G. L., Ackerman, A. S., Aleinov, I., Bauer, M., Bleck, R., Canuto, V., Cesana, G., Cheng, Y., Clune, T. L., Cook, B. I., Cruz, C. A., Del Genio, A. D., Elsaesser, G. S., Faluvegi, G., Kiang, N. Y., Kim, D., Lacs, A. A., Leboissetier, A., LeGrande, A. N., Lo, K. K., Marshall, J., Matthews, E. E., McDermid, S., Mezzuman, K., Miller, R. L., Murray, L. T., Oinas, V., Orbe, C., Garcia-Pando, C. P., Perlwitz, J. P., Puma, M. J., Rind, D., Romanou, A., Shindell, D. T., Sun, S., Tausnev, N., Tsigaridis, K., Tselioudis, G., Weng, E., Wu, J., and Yao, M.: GISS-E2.1: Configurations and Climatology, *J Adv Model Earth Syst*, 12, e2019MS002025, <https://doi.org/10.1029/2019MS002025>, 2020.

Kessler, W. S.: EOF Representations of the Madden–Julian Oscillation and Its Connection with ENSO, *J. Climate*, 14, 3055–3061, [https://doi.org/10.1175/1520-0442\(2001\)014<3055:EROTMJ>2.0.CO;2](https://doi.org/10.1175/1520-0442(2001)014<3055:EROTMJ>2.0.CO;2), 2001.

- 1619 Kiladis, G. N., Wheeler, M. C., Haertel, P. T., Straub, K. H., and Roundy, P. E.: Convectively coupled equatorial waves,
 1620 *Reviews of Geophysics*, 47, 2008RG000266, <https://doi.org/10.1029/2008RG000266>, 2009.
 1621
- 1622 Kim, D., Xavier, P., Maloney, E., Wheeler, M., Waliser, D., Sperber, K., Hendon, H., Zhang, C., Neale, R., Hwang, Y.-T., and
 1623 Liu, H.: Process-Oriented MJO Simulation Diagnostic: Moisture Sensitivity of Simulated Convection, *Journal of Climate*, 27,
 1624 5379–5395, <https://doi.org/10.1175/JCLI-D-13-00497.1>, 2014.
 1625
- 1626 Kim, H., Caron, J. M., Richter, J. H., and Simpson, I. R.: The Lack of QBO-MJO Connection in CMIP6 Models, *Geophysical*
 1627 *Research Letters*, 47, e2020GL087295, <https://doi.org/10.1029/2020GL087295>, 2020.
 1628
- 1629 Kim, J., K. M. Grise, and S.-W. Son, 2013: Thermal characteristics of the cold-point tropopause region in CMIP5 models,
 1630 *Journal of Geophysical Research - Atmospheres*, 118, 8827-8841.
 1631
- 1632 Klotzbach, P., Abhik, S., Hendon, H. H., Bell, M., Lucas, C., G. Marshall, A., and Oliver, E. C. J.: On the emerging relationship
 1633 between the stratospheric Quasi-Biennial oscillation and the Madden-Julian oscillation, *Sci Rep*, 9, 2981,
 1634 <https://doi.org/10.1038/s41598-019-40034-6>, 2019.
 1635
- 1636 Kumar, V., Yoden, S., and Hitchman, M. H.: QBO and ENSO Effects on the Mean Meridional Circulation, Polar Vortex,
 1637 Subtropical Westerly Jets, and Wave Patterns During Boreal Winter, *JGR Atmospheres*, 127,
 1638 e2022JD036691, <https://doi.org/10.1029/2022JD036691>, 2022.
 1639
- 1640 Lawrence, Z. D., Elsbury, D., Butler, A. H., Perlwitz, J., Albers, J. R., Ciasto, L. M., and Ray, E.: Evaluation of Processes
 1641 Related to Stratosphere–Troposphere Coupling in GEFsv12 Subseasonal Hindcasts, *Monthly Weather Review*, 151, 1735–
 1642 1755, <https://doi.org/10.1175/MWR-D-22-0283.1>, 2023.
 1643 [Liebmann, B., and Smith, C. A.: Description of a Complete \(Interpolated\) Outgoing Longwave Radiation Dataset, *Bulletin of*](#)
 1644 [the American Meteorological Society](#) 77, 6, 1274–78. <https://doi.org/10.1175/1520-0477-77.6.1274>, 1996.
 1645
- 1646 Lim, Y. and Son, S.: QBO-MJO Connection in CMIP5 Models, *JGR Atmospheres*, 125, e2019JD032157,
 1647 <https://doi.org/10.1029/2019JD032157>, 2020.
 1648
- 1649 Lin, H.: The Madden-Julian Oscillation, *Atmosphere-Ocean*, 60, 338–359, <https://doi.org/10.1080/07055900.2022.2072267>,
 1650 2022.
 1651
- 1652 Madden, R. A. and Julian, P. R.: Observations of the 40–50-Day Tropical Oscillation—A Review, *Mon. Wea. Rev.*, 122, 814–
 1653 837, [https://doi.org/10.1175/1520-0493\(1994\)122<0814:OOTDIO>2.0.CO;2](https://doi.org/10.1175/1520-0493(1994)122<0814:OOTDIO>2.0.CO;2), 1994.
 1654
- 1655 Martin, Z., S.-W. Son, A. Butler, H. Hendon, H. Kim, A. Sobel, S. Yoden, and C. Zhang, 2021: The influence of the Quasi-
 1656 Biennial Oscillation on the Madden-Julian Oscillation, *Nature Reviews Earth & Environment*, <https://doi.org/10.1038/s43017-021-00173-9>.
 1657
- 1658
- 1659 Martin, Z. K., Simpson, I. R., Lin, P., Orbe, C., Tang, Q., Caron, J. M., Chen, C., Kim, H., Leung, L. R., Richter, J. H., and
 1660 Xie, S.: The Lack of a QBO-MJO Connection in Climate Models With a Nudged Stratosphere, *JGR Atmospheres*, 128,
 1661 e2023JD038722, <https://doi.org/10.1029/2023JD038722>, 2023.
 1662
- 1663 Matsuno, T.: Quasi-Geostrophic Motions in the Equatorial Area, *Journal of the Meteorological Society of Japan*, 44, 25–43,
 1664 https://doi.org/10.2151/jmsj1965.44.1_25, 1966.
 1665
- 1666 Miura, H., Maeda, T., and Kimoto, M.: A Comparison of the Madden-Julian Oscillation Simulated by Different Versions of
 1667 the MIROC Climate Model, *SOLA*, 8, 165–169, <https://doi.org/10.2151/sola.2012-040>, 2012.
 1668

1669 Nakamura, Y. and Takayabu, Y. N.: Convective Couplings with Equatorial Rossby Waves and Equatorial Kelvin Waves. Part
 1670 I: Coupled Wave Structures, *Journal of the Atmospheric Sciences*, 79, 247–262, <https://doi.org/10.1175/JAS-D-21-0080.1>,
 1671 2022.

1672
 1673 [Naoe, H., Garcia-Franco, J. L., Park, C.-H., Rodrigo, M., Palmeiro, F. M., Serva, F., Taguchi, M., Yoshida, K., Anstey, J. A.,
 1674 Garcia-Serrano, J., Son, S.-W., Kawatani, Y., Butchart, N., Hamilton, K., Chen, C.-C., Glanville, A., Kerzenmacher, T., Lott,
 1675 F., Orbe, C., Osprey, S., Park, M., Richter, J. H., Versick, S., and Watanabe, S.: QBOi El Niño Southern Oscillation
 1676 experiments: Teleconnections of the QBO, EGUsphere \[preprint\]. <https://doi.org/10.5194/egusphere-2025-1148>, 2025.](#)

1677
 1678 Newman, M., Sardeshmukh, P. D., and Penland, C.: How Important Is Air–Sea Coupling in ENSO and MJO Evolution?,
 1679 *Journal of Climate*, 22, 2958–2977, <https://doi.org/10.1175/2008JCLI2659.1>, 2009.

1680
 1681 Nordeng, T.-E.: Extended versions of the convective parametrization scheme at ECMWF and their impact on the mean and
 1682 transient activity of the model in the tropics, <https://doi.org/10.21957/E34XWHYSW>, 1994.

1683
 1684 [Orbe, C., Van Roekel, L., Adames, Á. F., Dezfali, A., Fasullo, J., Gleckler, P. J., Lee, J., Li, W., Nazarenko, L., Schmidt, G.,
 1685 A., Sperber, K. R., & Zhao, M.: Representation of Modes of Variability in Six U.S. Climate Models, *Journal of Climate*,
 1686 33\(17\), 7591–7617. <https://doi.org/10.1175/JCLI-D-19-0956.1>, 2020.](#)

1687
 1688 Pahlavan, H. A., Wallace, J. M., Fu, Q., and Kiladis, G. N.: Revisiting the Quasi-Biennial Oscillation as Seen in ERA5. Part
 1689 II: Evaluation of Waves and Wave Forcing, *Journal of the Atmospheric Sciences*, 78, 693–707, [https://doi.org/10.1175/JAS-
 1691 D-20-0249.1](https://doi.org/10.1175/JAS-

 1690 D-20-0249.1), 2021.

1692 Pan, D. and Randall, D. D. A.: A cumulus parameterization with a prognostic closure, *Quart J Royal Meteorol Soc*, 124, 949–
 1693 981, <https://doi.org/10.1002/qj.49712454714>, 1998.

1694
 1695 Pang, B., Chen, Z., Wen, Z., and Lu, R.: Impacts of two types of El Niño on the MJO during boreal winter, *Adv. Atmos. Sci.*,
 1696 33, 979–986, <https://doi.org/10.1007/s00376-016-5272-2>, 2016.

1697
 1698 Pascoe, C. L., Gray, L. J., Crooks, S. A., Jukes, M. N., and Baldwin, M. P.: The quasi-biennial oscillation: Analysis using
 1699 ERA-40 data, *J. Geophys. Res.*, 110, 2004JD004941, <https://doi.org/10.1029/2004JD004941>, 2005.

1700
 1701 Philander, S. G.: *El Niño, La Niña, and the southern oscillation*, Academic Press, San Diego, 293 pp., 1990.

1702
 1703 Pohl, B. and Matthews, A. J.: Observed Changes in the Lifetime and Amplitude of the Madden–Julian Oscillation Associated
 1704 with Interannual ENSO Sea Surface Temperature Anomalies, *Journal of Climate*, 20, 2659–2674,
 1705 <https://doi.org/10.1175/JCLI4230.1>, 2007.

1706
 1707 Puy, M., Vialard, J., Lengaigne, M., and Guilyardi, E.: Modulation of equatorial Pacific westerly/easterly wind events by the
 1708 Madden–Julian oscillation and convectively-coupled Rossby waves, *Clim Dyn*, 46, 2155–2178,
 1709 <https://doi.org/10.1007/s00382-015-2695-x>, 2016.

1710
 1711 Randall, D. A., Tziperman, E., Branson, M. D., Richter, J. H., and Kang, W.: The QBO–MJO Connection: A Possible Role
 1712 for the SST and ENSO, *Journal of Climate*, 36, 6515–6531, <https://doi.org/10.1175/JCLI-D-23-0031.1>, 2023.

1713
 1714 Richter, J. H., Anstey, J. A., Butchart, N., Kawatani, Y., Meehl, G. A., Osprey, S., and Simpson, I. R.: Progress in Simulating
 1715 the Quasi-Biennial Oscillation in CMIP Models, *JGR Atmospheres*, 125, e2019JD032362,
 1716 <https://doi.org/10.1029/2019JD032362>, 2020.

- 1718 Rind, D., Jonas, J., Balachandran, N. K., Schmidt, G. A., and Lean, J.: The QBO in two GISS global climate models: 1.
1719 Generation of the QBO, *JGR Atmospheres*, 119, 8798–8824, <https://doi.org/10.1002/2014JD021678>, 2014.
1720
- 1721 Rind, D., Orbe, C., Jonas, J., Nazarenko, L., Zhou, T., Kelley, M., Lacis, A., Shindell, D., Faluvegi, G., Romanou, A., Russell,
1722 G., Tausnev, N., Bauer, M., and Schmidt, G.: GISS Model E2.2: A Climate Model Optimized for the Middle Atmosphere—
1723 Model Structure, Climatology, Variability, and Climate Sensitivity, *JGR Atmospheres*, 125, e2019JD032204,
1724 <https://doi.org/10.1029/2019JD032204>, 2020.
1725
- 1726 Roundy, P. E.: The Spectrum of Convectively Coupled Kelvin Waves and the Madden–Julian Oscillation in Regions of Low-
1727 Level Easterly and Westerly Background Flow, *Journal of the Atmospheric Sciences*, 69, 2107–2111,
1728 <https://doi.org/10.1175/JAS-D-12-060.1>, 2012.
1729
- 1730 Sakaeda, N., Dias, J., and Kiladis, G. N.: The Unique Characteristics and Potential Mechanisms of the MJO-QBO Relationship,
1731 *JGR Atmospheres*, 125, e2020JD033196, <https://doi.org/10.1029/2020JD033196>, 2020.
1732
- 1733 Schenzinger, V., Osprey, S., Gray, L., and Butchart, N.: Defining metrics of the Quasi-Biennial Oscillation in global climate
1734 models, *Geosci. Model Dev.*, 10, 2157–2168, <https://doi.org/10.5194/gmd-10-2157-2017>, 2017.
1735
- 1736 Schreck, C. J.: Global Survey of the MJO and Extreme Precipitation, *Geophysical Research Letters*, 48,
1737 e2021GL094691, <https://doi.org/10.1029/2021GL094691>, 2021.
1738
- 1739 Serva, F., Anstey, J. A., Bushell, A. C., Butchart, N., Cagnazzo, C., Gray, L. J., Kawatani, Y., Osprey, S. M., Richter, J. H.,
1740 and Simpson, I. R.: The impact of the QBO on the region of the tropical tropopause in QBOi models: Present-day simulations,
1741 *Quart J Royal Meteorol Soc*, 148, 1945–1964, <https://doi.org/10.1002/qj.4287>, 2022.
1742
- 1743 Serva, F., Christiansen, B., Davini, P., Von Hardenberg, J., Van Den Oord, G., Reerink, T. J., Wyser, K., and Yang, S.: Changes
1744 in Stratospheric Dynamics Simulated by the EC-Earth Model From CMIP5 to CMIP6, *J Adv Model Earth Syst*, 16,
1745 e2023MS003756, <https://doi.org/10.1029/2023MS003756>, 2024.
1746
- 1747 Slingo, J. M., Rowell, D. P., Sperber, K. R., and Nortley, F.: On the predictability of the interannual behaviour of the Madden-
1748 Julian oscillation and its relationship with el Niño, *Quart J Royal Meteorol Soc*, 125, 583–609,
1749 <https://doi.org/10.1002/qj.49712555411>, 1999.
1750
- 1751 Son, S.-W., Lim, Y., Yoo, C., Hendon, H. H., and Kim, J.: Stratospheric Control of the Madden–Julian Oscillation, *Journal of*
1752 *Climate*, 30, 1909–1922, <https://doi.org/10.1175/JCLI-D-16-0620.1>, 2017.
1753
- 1754 Straub, K. H. and Kiladis, G. N.: Observations of a Convectively Coupled Kelvin Wave in the Eastern Pacific ITCZ, *J. Atmos.*
1755 *Sci.*, 59, 30–53, [https://doi.org/10.1175/1520-0469\(2002\)059<0030:OOACCK>2.0.CO;2](https://doi.org/10.1175/1520-0469(2002)059<0030:OOACCK>2.0.CO;2), 2002.
1756
- 1757 Suematsu, T. and Miura, H.: Zonal SST Difference as a Potential Environmental Factor Supporting the Longevity of the
1758 Madden–Julian Oscillation, *Journal of Climate*, 31, 7549–7564, <https://doi.org/10.1175/JCLI-D-17-0822.1>, 2018.
1759
- 1760 Suematsu, T. and Miura, H.: Changes in the Eastward Movement Speed of the Madden–Julian Oscillation with Fluctuation in
1761 the Walker Circulation, *Journal of Climate*, 35, 211–225, <https://doi.org/10.1175/JCLI-D-21-0269.1>, 2022.
1762
- 1763 Sun, L., Wang, H., and Liu, F.: Combined effect of the QBO and ENSO on the MJO, *Atmospheric and Oceanic Science*
1764 *Letters*, 12, 170–176, <https://doi.org/10.1080/16742834.2019.1588064>, 2019.
1765
- 1766 Tam, C.-Y. and Lau, N.-C.: Modulation of the Madden-Julian Oscillation by ENSO: Inferences from Observations and GCM
1767 Simulations, *Journal of the Meteorological Society of Japan*, 83, 727–743, <https://doi.org/10.2151/jmsj.83.727>, 2005.

- 1768
1769 Tegtmeier, S., Anstey, J., Davis, S., Ivanciu, I., Jia, Y., McPhee, D., and Pilch Kedzierski, R.: Zonal Asymmetry of the QBO
1770 Temperature Signal in the Tropical Tropopause Region, *Geophysical Research Letters*, 47, e2020GL089533,
1771 <https://doi.org/10.1029/2020GL089533>, 2020.
- 1772
1773 Tiedtke, M.: A Comprehensive Mass Flux Scheme for Cumulus Parameterization in Large-Scale Models, *Mon. Wea. Rev.*,
1774 117, 1779–1800, [https://doi.org/10.1175/1520-0493\(1989\)117<1779:ACMFSF>2.0.CO;2](https://doi.org/10.1175/1520-0493(1989)117<1779:ACMFSF>2.0.CO;2), 1989.
- 1775
1776 Vitart, F.: Madden—Julian Oscillation prediction and teleconnections in the S2S database, *Quart J Royal Meteor Soc*, 143,
1777 2210–2220, <https://doi.org/10.1002/qj.3079>, 2017.
- 1778
1779 Waliser, D., Sperber, K., Hendon, H., Kim, D., Maloney, E., Wheeler, M., Weickmann, K., Zhang, C., Donner, L., Gottschalck,
1780 J. and Higgins, W. MJO simulation diagnostics. *J. Climate*, 22, 3006–3030, <https://doi.org/10.1175/2008JCLI2731.1>, 2009
- 1781
1782 Wang, B., Chen, G., and Liu, F.: Diversity of the Madden-Julian Oscillation, *Sci. Adv.*, 5, eaax0220,
1783 <https://doi.org/10.1126/sciadv.aax0220>, 2019.
- 1784
1785 Wang, T. and Li, T.: Diversity of MJO Initiation Regions and Processes, *Journal of Climate*, 35, 3121–3140,
1786 <https://doi.org/10.1175/JCLI-D-21-0816.1>, 2022.
- 1787
1788 Wang, Y.-C., Tseng, W.-L., and Hsu, H.-H.: Role of convection–circulation coupling in the propagation mechanism of the
1789 Madden–Julian Oscillation over the Maritime Continent in a climate model, *Clim Dyn*, 58, 2469–2484,
1790 <https://doi.org/10.1007/s00382-021-06013-2>, 2022.
- 1791
1792 Wei, Y. and Ren, H.-L.: Modulation of ENSO on Fast and Slow MJO Modes during Boreal Winter, *Journal of Climate*, 32,
1793 7483–7506, <https://doi.org/10.1175/JCLI-D-19-0013.1>, 2019.
- 1794
1795 Wheeler, M. C. and Hendon, H. H.: An All-Season Real-Time Multivariate MJO Index: Development of an Index for
1796 Monitoring and Prediction, *Mon. Wea. Rev.*, 132, 1917–1932, [https://doi.org/10.1175/1520-0493\(2004\)132<1917:AARMMI>2.0.CO;2](https://doi.org/10.1175/1520-0493(2004)132<1917:AARMMI>2.0.CO;2), 2004.
- 1797
1798
1799 Yadav, P. and Straus, D. M.: Circulation Response to Fast and Slow MJO Episodes, *Monthly Weather Review*, 145, 1577–
1800 1596, <https://doi.org/10.1175/MWR-D-16-0352.1>, 2017.
- 1801
1802 Yadav, P., Garfinkel, C. I., and Domeisen, D. I. V.: The Role of the Stratosphere in Teleconnections Arising From Fast and
1803 Slow MJO Episodes, *Geophysical Research Letters*, 51, e2023GL104826, <https://doi.org/10.1029/2023GL104826>, 2024.
- 1804
1805 Yoo, C., and S.-W. Son, 2016: Modulation of the boreal wintertime Madden-Julian Oscillation by the stratospheric Quasi-
1806 Biennial Oscillation, *Geophysical Research Letters*, 43, 1392–1398.
- 1807
1808 Yukimoto, S., Kawai, H., Koshiro, T., Oshima, N., Yoshida, K., Urakawa, S., Tsujino, H., Deushi, M., Tanaka, T., Hosaka,
1809 M., Yabu, S., Yoshimura, H., Shindo, E., Mizuta, R., Obata, A., Adachi, Y., and Ishii, M.: The Meteorological Research
1810 Institute Earth System Model Version 2.0, MRI-ESM2.0: Description and Basic Evaluation of the Physical Component,
1811 *Journal of the Meteorological Society of Japan*, 97, 931–965, <https://doi.org/10.2151/jmsj.2019-051>, 2019.
- 1812
1813 Yuni, A. R. E., Lubis, S. W., and Setiawan, S.: Vertical structure of Convectively Coupled Equatorial Waves (CCEWs) during
1814 Boreal Summer and Winter, *IOP Conf. Ser.: Earth Environ. Sci.*, 284, 012010, <https://doi.org/10.1088/1755-1315/284/1/012010>, 2019.
- 1815
1816

1817 Zhang, C. and Gottschalck, J.: SST Anomalies of ENSO and the Madden–Julian Oscillation in the Equatorial Pacific*, J.
1818 Climate, 15, 2429–2445, [https://doi.org/10.1175/1520-0442\(2002\)015<2429:SAOEAT>2.0.CO;2](https://doi.org/10.1175/1520-0442(2002)015<2429:SAOEAT>2.0.CO;2), 2002.

1819
1820 Zhang, G. J. and McFarlane, N. A.: Sensitivity of climate simulations to the parameterization of cumulus convection in the
1821 Canadian climate centre general circulation model, Atmosphere-Ocean, 33, 407–446,
1822 <https://doi.org/10.1080/07055900.1995.9649539>, 1995.

1823
1824 Zhu, J., Kumar, A., and Wang, W.: Dependence of MJO Predictability on Convective Parameterizations, Journal of Climate,
1825 33, 4739–4750, <https://doi.org/10.1175/JCLI-D-18-0552.1>, 2020.

1826
1827

Page 1: [1] Formatted **DE** **9/2/25 11:04:00 PM**

Header

Page 6: [2] Commented [FS1] **FEDERICO SERVA** **8/22/25 12:01:00 PM**

I've changed the vertical column a bit to avoid repetition

Page 6: [3] Deleted **DE** **9/2/25 11:04:00 PM**

Page 6: [3] Deleted **DE** **9/2/25 11:04:00 PM**

Page 6: [4] Formatted Table **DE** **9/2/25 11:04:00 PM**

Formatted Table

Page 6: [5] Formatted **DE** **9/2/25 11:04:00 PM**

Font color: Text 1

Page 6: [6] Formatted **DE** **9/2/25 11:04:00 PM**

Font color: Text 1

Page 6: [6] Formatted **DE** **9/2/25 11:04:00 PM**

Font color: Text 1

Page 6: [7] Formatted **DE** **9/2/25 11:04:00 PM**

Font color: Text 1

Page 6: [7] Formatted **DE** **9/2/25 11:04:00 PM**

Font color: Text 1

Page 6: [8] Formatted **DE** **9/2/25 11:04:00 PM**

Font color: Text 1

Page 6: [9] Formatted **DE** **9/2/25 11:04:00 PM**

Font color: Text 1

Page 6: [10] Formatted **DE** **9/2/25 11:04:00 PM**

Font: +Body (Cambria), Font color: Text 1

Page 6: [11] Formatted **DE** **9/2/25 11:04:00 PM**

Font color: Text 1

Page 6: [11] Formatted **DE** **9/2/25 11:04:00 PM**

Font color: Text 1

Page 6: [12] Formatted	DE	9/2/25 11:04:00 PM
-------------------------------	-----------	---------------------------

Font color: Text 1

Page 6: [13] Formatted	DE	9/2/25 11:04:00 PM
-------------------------------	-----------	---------------------------

Font color: Text 1

Page 6: [14] Formatted	DE	9/2/25 11:04:00 PM
-------------------------------	-----------	---------------------------

Font: +Body (Cambria), Font color: Text 1

Page 6: [15] Formatted	DE	9/2/25 11:04:00 PM
-------------------------------	-----------	---------------------------

Font color: Text 1

Page 6: [15] Formatted	DE	9/2/25 11:04:00 PM
-------------------------------	-----------	---------------------------

Font color: Text 1

Page 6: [16] Formatted	DE	9/2/25 11:04:00 PM
-------------------------------	-----------	---------------------------

Font color: Text 1

Page 6: [17] Formatted	DE	9/2/25 11:04:00 PM
-------------------------------	-----------	---------------------------

Font color: Text 1

Page 6: [18] Formatted	DE	9/2/25 11:04:00 PM
-------------------------------	-----------	---------------------------

Font: +Body (Cambria), Font color: Text 1

Page 6: [19] Formatted	DE	9/2/25 11:04:00 PM
-------------------------------	-----------	---------------------------

Font color: Text 1

Page 6: [19] Formatted	DE	9/2/25 11:04:00 PM
-------------------------------	-----------	---------------------------

Font color: Text 1

Page 6: [20] Formatted	DE	9/2/25 11:04:00 PM
-------------------------------	-----------	---------------------------

Font color: Text 1

Page 6: [21] Formatted	DE	9/2/25 11:04:00 PM
-------------------------------	-----------	---------------------------

Font color: Text 1

Page 6: [22] Formatted	DE	9/2/25 11:04:00 PM
-------------------------------	-----------	---------------------------

Font: +Body (Cambria), Font color: Text 1

Page 6: [23] Formatted	DE	9/2/25 11:04:00 PM
-------------------------------	-----------	---------------------------

Font color: Text 1

Page 6: [23] Formatted	DE	9/2/25 11:04:00 PM
-------------------------------	-----------	---------------------------

Font color: Text 1

Page 6: [24] Formatted	DE	9/2/25 11:04:00 PM
-------------------------------	-----------	---------------------------

Font color: Text 1

Page 6: [25] Formatted	DE	9/2/25 11:04:00 PM
-------------------------------	-----------	---------------------------

Font color: Text 1

Page 6: [26] Formatted	DE	9/2/25 11:04:00 PM
-------------------------------	-----------	---------------------------

Font: +Body (Cambria), Font color: Text 1

Page 6: [27] Formatted	DE	9/2/25 11:04:00 PM
-------------------------------	-----------	---------------------------

Font color: Text 1

Page 6: [27] Formatted	DE	9/2/25 11:04:00 PM
-------------------------------	-----------	---------------------------

Font color: Text 1

Page 6: [28] Formatted	DE	9/2/25 11:04:00 PM
-------------------------------	-----------	---------------------------

Font color: Text 1

Page 6: [29] Formatted	DE	9/2/25 11:04:00 PM
-------------------------------	-----------	---------------------------

Font color: Text 1

Page 6: [30] Formatted	DE	9/2/25 11:04:00 PM
-------------------------------	-----------	---------------------------

Font: +Body (Cambria), Font color: Text 1

Page 6: [31] Formatted	DE	9/2/25 11:04:00 PM
-------------------------------	-----------	---------------------------

Font color: Text 1

Page 6: [31] Formatted	DE	9/2/25 11:04:00 PM
-------------------------------	-----------	---------------------------

Font color: Text 1

Page 6: [32] Formatted	DE	9/2/25 11:04:00 PM
-------------------------------	-----------	---------------------------

Font color: Text 1

Page 6: [33] Formatted	DE	9/2/25 11:04:00 PM
-------------------------------	-----------	---------------------------

Font color: Text 1

Page 6: [34] Formatted	DE	9/2/25 11:04:00 PM
-------------------------------	-----------	---------------------------

Font: +Body (Cambria), Font color: Text 1

Page 6: [35] Formatted	DE	9/2/25 11:04:00 PM
-------------------------------	-----------	---------------------------

Font color: Text 1

Page 6: [35] Formatted	DE	9/2/25 11:04:00 PM
-------------------------------	-----------	---------------------------

Font color: Text 1

Page 6: [36] Formatted	DE	9/2/25 11:04:00 PM
-------------------------------	-----------	---------------------------

Font color: Text 1

Page 6: [37] Formatted	DE	9/2/25 11:04:00 PM
-------------------------------	-----------	---------------------------

Font color: Text 1

Page 6: [38] Formatted	DE	9/2/25 11:04:00 PM
-------------------------------	-----------	---------------------------

Font color: Text 1

Page 6: [38] Formatted	DE	9/2/25 11:04:00 PM
-------------------------------	-----------	---------------------------

Font color: Text 1

Page 6: [39] Formatted	DE	9/2/25 11:04:00 PM
-------------------------------	-----------	---------------------------

Font color: Text 1

Page 6: [40] Formatted	DE	9/2/25 11:04:00 PM
-------------------------------	-----------	---------------------------

Font color: Text 1

Page 6: [41] Formatted	DE	9/2/25 11:04:00 PM
-------------------------------	-----------	---------------------------

Font: +Body (Cambria), Font color: Text 1

Page 6: [42] Deleted	DE	9/2/25 11:04:00 PM
-----------------------------	-----------	---------------------------

▼

Page 6: [42] Deleted	DE	9/2/25 11:04:00 PM
-----------------------------	-----------	---------------------------

▼

Page 8: [43] Deleted	DE	9/2/25 11:04:00 PM
-----------------------------	-----------	---------------------------

▼

Page 8: [43] Deleted	DE	9/2/25 11:04:00 PM
-----------------------------	-----------	---------------------------

▼

Page 8: [43] Deleted	DE	9/2/25 11:04:00 PM
-----------------------------	-----------	---------------------------

▼

Page 8: [43] Deleted	DE	9/2/25 11:04:00 PM
----------------------	----	--------------------

▼

Page 8: [43] Deleted	DE	9/2/25 11:04:00 PM
----------------------	----	--------------------

▼

Page 8: [43] Deleted	DE	9/2/25 11:04:00 PM
----------------------	----	--------------------

▼

Page 8: [43] Deleted	DE	9/2/25 11:04:00 PM
----------------------	----	--------------------

▼

Page 8: [43] Deleted	DE	9/2/25 11:04:00 PM
----------------------	----	--------------------

▼

Page 8: [43] Deleted	DE	9/2/25 11:04:00 PM
----------------------	----	--------------------

▼

Page 8: [43] Deleted	DE	9/2/25 11:04:00 PM
----------------------	----	--------------------

▼

Page 8: [44] Deleted	DE	9/2/25 11:04:00 PM
----------------------	----	--------------------

▼

Page 8: [44] Deleted	DE	9/2/25 11:04:00 PM
----------------------	----	--------------------

▼

Page 8: [44] Deleted	DE	9/2/25 11:04:00 PM
----------------------	----	--------------------

▼

Page 8: [44] Deleted	DE	9/2/25 11:04:00 PM
----------------------	----	--------------------

▼

Page 8: [44] Deleted	DE	9/2/25 11:04:00 PM
----------------------	----	--------------------

▼

Page 8: [44] Deleted	DE	9/2/25 11:04:00 PM
----------------------	----	--------------------

▼

Page 8: [44] Deleted	DE	9/2/25 11:04:00 PM
----------------------	----	--------------------

▼

Page 8: [44] Deleted	DE	9/2/25 11:04:00 PM
----------------------	----	--------------------

▼

Page 8: [44] Deleted	DE	9/2/25 11:04:00 PM
----------------------	----	--------------------

▼

Page 8: [44] Deleted	DE	9/2/25 11:04:00 PM
----------------------	----	--------------------

▼

Page 8: [44] Deleted	DE	9/2/25 11:04:00 PM
----------------------	----	--------------------

▼

Page 8: [44] Deleted	DE	9/2/25 11:04:00 PM
----------------------	----	--------------------

▼

Page 8: [44] Deleted	DE	9/2/25 11:04:00 PM
----------------------	----	--------------------

▼

Page 8: [44] Deleted	DE	9/2/25 11:04:00 PM
----------------------	----	--------------------

▼

Page 8: [44] Deleted	DE	9/2/25 11:04:00 PM
----------------------	----	--------------------

▼

Page 8: [44] Deleted	DE	9/2/25 11:04:00 PM
----------------------	----	--------------------

▼

Page 8: [44] Deleted	DE	9/2/25 11:04:00 PM
----------------------	----	--------------------

▼

Page 8: [44] Deleted	DE	9/2/25 11:04:00 PM
----------------------	----	--------------------

▼

Page 8: [44] Deleted	DE	9/2/25 11:04:00 PM
----------------------	----	--------------------

▼

Page 8: [44] Deleted	DE	9/2/25 11:04:00 PM
----------------------	----	--------------------

▼

Page 8: [44] Deleted	DE	9/2/25 11:04:00 PM
----------------------	----	--------------------

▼.....

Page 8: [44] Deleted	DE	9/2/25 11:04:00 PM
-----------------------------	-----------	---------------------------

▼.....

Page 8: [44] Deleted	DE	9/2/25 11:04:00 PM
-----------------------------	-----------	---------------------------

▼.....

Page 8: [44] Deleted	DE	9/2/25 11:04:00 PM
-----------------------------	-----------	---------------------------

▼.....

Page 8: [44] Deleted	DE	9/2/25 11:04:00 PM
-----------------------------	-----------	---------------------------

▼.....

Page 15: [45] Deleted	DE	9/2/25 11:04:00 PM
------------------------------	-----------	---------------------------

▼.....

Page 15: [45] Deleted	DE	9/2/25 11:04:00 PM
------------------------------	-----------	---------------------------

▼.....

Page 15: [45] Deleted	DE	9/2/25 11:04:00 PM
------------------------------	-----------	---------------------------

▼.....

Page 15: [46] Deleted	DE	9/2/25 11:04:00 PM
------------------------------	-----------	---------------------------

▼.....

Page 15: [46] Deleted	DE	9/2/25 11:04:00 PM
------------------------------	-----------	---------------------------

▼.....

Page 15: [46] Deleted	DE	9/2/25 11:04:00 PM
------------------------------	-----------	---------------------------

▼.....

Page 15: [46] Deleted	DE	9/2/25 11:04:00 PM
------------------------------	-----------	---------------------------

▼.....

Page 15: [46] Deleted	DE	9/2/25 11:04:00 PM
------------------------------	-----------	---------------------------

▼.....

Page 16: [47] Deleted	DE	9/2/25 11:04:00 PM
------------------------------	-----------	---------------------------

▼.....

Page 16: [47] Deleted	DE	9/2/25 11:04:00 PM
------------------------------	-----------	---------------------------

Page 16: [47] Deleted DE 9/2/25 11:04:00 PM

Page 16: [48] Deleted DE 9/2/25 11:04:00 PM

Page 16: [49] Commented [de14R12] delsbury@uci.edu 8/28/25 12:09:00 PM

▼.....
Page 19: [51] Deleted **DE** **9/2/25 11:04:00 PM**

▼.....
Page 19: [51] Deleted **DE** **9/2/25 11:04:00 PM**

▼.....
Page 19: [51] Deleted **DE** **9/2/25 11:04:00 PM**

▼.....
Page 19: [51] Deleted **DE** **9/2/25 11:04:00 PM**

▼.....
Page 19: [51] Deleted **DE** **9/2/25 11:04:00 PM**

▼.....
Page 19: [51] Deleted **DE** **9/2/25 11:04:00 PM**

▼.....
Page 19: [51] Deleted **DE** **9/2/25 11:04:00 PM**

▼.....
Page 19: [51] Deleted **DE** **9/2/25 11:04:00 PM**

▼.....
Page 19: [51] Deleted **DE** **9/2/25 11:04:00 PM**

▼.....
Page 19: [51] Deleted **DE** **9/2/25 11:04:00 PM**

▼.....
Page 19: [51] Deleted **DE** **9/2/25 11:04:00 PM**

▼.....
Page 19: [51] Deleted **DE** **9/2/25 11:04:00 PM**

▼.....
Page 19: [51] Deleted **DE** **9/2/25 11:04:00 PM**

▼.....
Page 19: [51] Deleted **DE** **9/2/25 11:04:00 PM**

▼.....
Page 19: [51] Deleted **DE** **9/2/25 11:04:00 PM**

▼.....
Page 19: [51] Deleted **DE** **9/2/25 11:04:00 PM**

▼.....
Page 19: [51] Deleted **DE** **9/2/25 11:04:00 PM**

▼.....
Page 19: [51] Deleted **DE** **9/2/25 11:04:00 PM**

▼.....
Page 19: [51] Deleted **DE** **9/2/25 11:04:00 PM**

▼.....
Page 19: [51] Deleted **DE** **9/2/25 11:04:00 PM**

▼.....
Page 19: [51] Deleted **DE** **9/2/25 11:04:00 PM**

▼.....
Page 19: [51] Deleted **DE** **9/2/25 11:04:00 PM**

▼.....
Page 19: [51] Deleted **DE** **9/2/25 11:04:00 PM**

▼.....
Page 19: [51] Deleted **DE** **9/2/25 11:04:00 PM**

▼.....
Page 19: [51] Deleted **DE** **9/2/25 11:04:00 PM**

▼.....
Page 19: [51] Deleted **DE** **9/2/25 11:04:00 PM**

▼.....
Page 19: [51] Deleted **DE** **9/2/25 11:04:00 PM**

▼.....
Page 19: [51] Deleted **DE** **9/2/25 11:04:00 PM**

▼.....
Page 19: [51] Deleted **DE** **9/2/25 11:04:00 PM**

▼.....
Page 19: [51] Deleted **DE** **9/2/25 11:04:00 PM**

▼.....
Page 19: [51] Deleted **DE** **9/2/25 11:04:00 PM**

▼.....
Page 19: [51] Deleted **DE** **9/2/25 11:04:00 PM**

▼.....
Page 19: [51] Deleted **DE** **9/2/25 11:04:00 PM**

▼.....
Page 19: [51] Deleted **DE** **9/2/25 11:04:00 PM**

▼.....
Page 19: [51] Deleted **DE** **9/2/25 11:04:00 PM**

▼.....
Page 19: [51] Deleted **DE** **9/2/25 11:04:00 PM**

▼.....
Page 19: [51] Deleted **DE** **9/2/25 11:04:00 PM**

▼.....
Page 19: [51] Deleted **DE** **9/2/25 11:04:00 PM**

▼.....
Page 19: [51] Deleted **DE** **9/2/25 11:04:00 PM**

▼.....
Page 19: [51] Deleted **DE** **9/2/25 11:04:00 PM**

▼.....
Page 19: [51] Deleted **DE** **9/2/25 11:04:00 PM**

▼.....
Page 19: [51] Deleted **DE** **9/2/25 11:04:00 PM**

▼.....
Page 19: [51] Deleted **DE** **9/2/25 11:04:00 PM**

▼.....
Page 19: [51] Deleted **DE** **9/2/25 11:04:00 PM**

▼.....
Page 19: [51] Deleted **DE** **9/2/25 11:04:00 PM**

▼.....
Page 19: [51] Deleted **DE** **9/2/25 11:04:00 PM**

▼.....
Page 21: [52] Deleted **DE** **9/2/25 11:04:00 PM**

▼.....
Page 21: [52] Deleted **DE** **9/2/25 11:04:00 PM**

▼.....
Page 23: [53] Deleted **DE** **9/2/25 11:04:00 PM**